NATIONAL ADVISORY COMMITTEE FOR AERONAUTICS

SPECIAL REPORT No. 118

[SAME AS TECH NOTE 976]

TESTS OF AIRFOILS DESIGNED TO DELAY THE COMPRESSIBILITY BURBLE

By John Stack
Langley Memorial Aeronautical Laboratory

June 1939

TESTS OF AIRFOILS DESIGNED TO DELAY THE COMPRESSIBILITY BURBLE

By John Stack

INTRODUCTION

Development of airfoil sections suitable for high-speed applications has generally been difficult because little was known of the flow phenomenon that occurs at high speeds. A definite critical speed had been found at which serious detrimental flow changes occur that lead to serious losses in lift and large increases in drag. This flow phenomenon, called the compressibility burble, was originally a propeller problem, but with the development of higher speed aircraft serious consideration must be given other parts of the airplane. It is important to realize, however, that the propeller will continue to offer the most serious compressibility problems for two reasons: first, because its speed is higher than the speed of the airplane, and second, because structural requirements lead to thicker sections near the root.

Fundamental investigations of high-speed air-flow phenomenon recently completed (references 1, 2, and 3) have provided much new information. From the practical standpoint an important conclusion of this work has been the determination of the critical speed, that is, the speed at which the compressibility burble occurs. The critical speed was shown to be the translational velocity at which the sum of the translational velocity and the maximum local induced velocity at the surface of the airfoil or other body equals the local speed of sound. Obviously then higher critical speeds can be attained through the development of airfoils that have minimum induced velocity for any given value of the lift coefficient.

Presumably, the highest critical speed will be attained by an airfoil that has uniform chordwise distribution of induced velocity or, in other words, a flat pressure-distribution curve. Normal airfoils all tend to have high negative pressures and correspondingly high induced velocities near the nose, gradually tapering off to the air-stream conditions at the rear of the airfoil. If the same lift coefficient can be obtained by decreasing the induced velocity near the nose and increasing the induced velocity over the after portion of the airfoil, the critical speed will be increased by an amount proportional to the decrease

obtained in the maximum induced velocity. The ideal airfoil for any given high-speed application is, then, that form which at its operating lift coefficient has uniform chordwise distribution of induced velocity. Accordingly, an analytical search for such airfoil forms has been conducted by members of the Laboratory staff and these forms are now being investigated experimentally in the 24-inch high-speed wind tunnel.

The first airfoils investigated showed marked improvement over those forms already available, not only as to critical speed but also the drag at low speeds is decreased considerably. Because of the marked improvement immediately achieved, it was considered desirable to extend the thickness and lift coefficient ranges for which the original forms had been designed to obtain data of immediate practical value before extending further the investigation of the fundamental aspects of the problem.

DEVELOPMENT OF AIRFOIL FORMS

The aerodynamic characteristics of any airfoil are in general dependent upon the airfoil camber line and the thickness form. For this series of airfoils, camber lines were derived analytically to obtain a uniform chordwise distribution of induced velocity or pressure for certain designated lift coefficients, and then an analytical search for a thickness form that likewise has low and uniform chordwise induced velocity distribution was undertaken.

Derivation of the camber line.- Glauert (reference 4) has derived expressions for the local induced velocity at a point on an airfoil (zero thickness assumed) in terms of the circulation around an airfoil, corresponding to a certain distribution of vorticity along the airfoil surface. By assuming the distribution of vorticity to be constant, a line airfoil is determined that gives uniform chordwise pressure distribution. The form of the equation so derived is

$$\frac{Y_c}{C_L} = \frac{1}{4\pi}\left[\log \frac{1}{1-x} + x \log \frac{1-x}{x}\right]$$

where Y_c is the ordinate of the camber line, x is the abscissa, and the chord length is taken as unity. This ideal form leads to discontinuities at the nose and tail

in the theoretical example. This difficulty is circumvented by assuming slight gradient in the chordwise load grading immediately at the nose and tail. This form derived by A. E. von Doenhoff of the Laboratory staff, using the Fourier series method, is given by the equation

$$\frac{Y_c}{C} = \frac{C_L}{4\pi}\left[0.3833 - 0.3333 \cos 2\theta - 0.0333 \cos 4\theta - 0.0095 \cos 6\theta - 0.0040 \cos 8\theta - 0.0020 \cos 10\theta - 0.0012 \cos 12\theta\right]$$

where $\frac{x}{c} = \frac{1}{2}(1 - \cos\theta)$ and c is the airfoil chord. This latter equation expresses the camber line chosen for airfoils of this series. Actually load or induced velocity gradings derived from both equations are identical for all practical purposes. Camber-line ordinates are given in table I for the value of $C_L = 1.0$. To obtain the camber line, giving uniform chordwise distribution of induced velocity for other values of the lift coefficient, the values given in table I are multiplied by the value of the desired lift coefficient.

Derivation of the thickness form.- The derivation of the thickness form is not as simple or direct as the derivation of the camber line. Theoretical pressure distribution was computed by the methods of reference 5 for each of the several forms investigated in reference 6. Some of these forms approached the desired form but further modifications were investigated analytically and finally two forms were chosen for tests. These forms and the pressure distribution for each are shown in figure 1. The complete airfoil profile is derived by first calculating the camber line for the desired lift coefficient and then in the usual manner lay out the thickness ordinates given in table II from the camber line.

Airfoil designation.- Because the ideal series of airfoils requires an extremely large variation of shape, it becomes practically impossible to use previous numbering systems and further, because this new series of airfoils is designed to obtain a specific pressure diagram, these airfoils are designated by a new series of numbers that are related to the flow and operating characteristics of the airfoil. The first digit represents a serial number that describes the class of pressure distribution, the

second number gives the location of the maximum negative pressure, and the numbers following the dash give the lift coefficient for which the airfoil was designed to operate and the airfoil thickness. Thus the 16-509 has the shape 16-009 disposed about the uniform chordwise load camber line designed for lift coefficient 0.5 and is 9 percent thick.

Airfoils investigated.- Two basic airfoil forms were investigated. These forms and the corresponding theoretical pressure-distribution diagrams are shown in figure 1. Theoretically the form N.A.C.A. 07-009 should give the higher critical speed but earlier investigation (reference 3) indicated that for pressures occurring near the leading edge, the increase in the pressure coefficient as a result of compressibility effects was greater than that for pressures occurring farther back on the airfoil. Consequently, it was believed that at speeds as high as the critical speed, the shape designated 07-009 might have as a result of compressibility effects a pressure peak near the leading edge. The form N.A.C.A. 16-009 was therefore developed as an attempt to achieve the uniform chordwise load distribution at high speeds. Both forms were tested and the results showed higher drag and lower critical speed for the N.A.C.A. 07-009 form. Accordingly, the form N.A.C.A. 16-009 was chosen as the basic form for a series of airfoils designed to operate at various lift coefficients. For one value of the lift coefficient the effect of thickness variation was also investigated. The airfoils tested are given in the following table and profiles are shown in figure 2.

N.A.C.A. 16-009	N.A.C.A. 16-506
N.A.C.A. 16-109	N.A.C.A. 16-512
N.A.C.A. 16-209	N.A.C.A. 16-515
N.A.C.A. 16-509	N.A.C.A. 16-521
N.A.C.A. 16-709	N.A.C.A. 16-530
N.A.C.A. 16-1009	N.A.C.A. 16-106
N.A.C.A. 07-009	N.A.C.A. 07-509

APPARATUS AND METHOD

The tests are being conducted in the N.A.C.A. 24-inch high-speed wind tunnel in which velocities approaching the speed of sound can be obtained. A brief description of this tunnel is given in reference 3. The balance measures lift drag and pitching moment and, except for improvements that permit a more accurate determination of the forces, is similar in principle to the one used in the 11-inch high-speed wind tunnel. The methods of operation are likewise similar to those employed in the operation of the 11-inch tunnel (reference 7).

The models are of 5-inch chord and 30-inch span and are made of duralumin. A complete description of the method of constructing the models is given in reference 8. The model mounting is similar to that used in the 11-inch tunnel (reference 7). The model extends across the tunnel and through holes, which are of the same shape as but slightly larger than the model, cut in flexible brass end plates that preserve the contour of the tunnel walls. The model ends are secured in the balance which extends half around the test section and is enclosed in the airtight tunnel chamber similar to the 11-inch tunnel installation (reference 7).

The speed range over which measurements were made extended, in general, from 25 percent of the speed of sound to values in excess of the critical speed. The corresponding Reynolds Number range was from approximately 700,000 to nearly 2,000,000. The lift coefficient range for which tests were made extends from zero lift for each airfoil to values approaching maximum lift. In making tests over such a large speed range, the range of forces becomes very large and, in order to preserve a high order of accuracy, the models are first tested over as wide a range as possible with the balance set for maximum sensitivity and then, by resetting the balance sensitivity, extending the range of forces measurable sufficiently to obtain the data corresponding to the large forces occurring at maximum lift. Maximum lift data are, therefore, not included in this preliminary report because the time required to obtain the data would materially delay the presentation of the data already available.

PRECISION

Accidental errors are indicated by the point scatter on the plots showing the measured test data. These are in general rather small and affect neither the application nor the comparison of the data. Tunnel effects arising from end leakage, restriction, and the usual type of tunnel-wall effect are important. Exact knowledge of these various effects is incomplete at the present time. The largest effects appear to arise from air leakage through the clearance between the model and the brass end plates in the tunnel wall through which the model passes. Investigations of the leakage effects have been made for the N.A.C.A. 0012 with a special type of internal gap or clearance that permitted wide variation of the gap. Data obtained with various gap settings from 0.01 inch up extrapolated to zero gap were used to evaluate the leakage correction for the standard-type mounting. These corrected data were then checked by means of wake survey drag measurements with end leakage eliminated by rubber seals. Because the balance chamber is airtight, the end leak condition is related to the pressure distribution around the model. It was therefore considered advisable to check the method of correction for end leak by wake survey tests with end leakage eliminated by rubber seals for these new airfoils which have radically different pressure distribution than the older forms like the N.A.C.A. 0012. Some of these data are shown in figure 3. In general, the agreement is excellent. Accordingly, the data have been corrected for end leakage effects.

Other tunnel effects have not been completely investigated and the data have not been corrected for such effects as restriction or the more usual type of wall effect. As presented, the data are therefore conservative inasmuch as investigations so far made indicate that the coefficients as presented in the figures are high and the critical speeds may be low. Strictly comparable data for two older airfoils are, however, included so that comparisons can be made.

DISCUSSION

Airfoil characteristics for several of the N.A.C.A. series 16 airfoils are given in figures 4 to 18. Examination of these figures indicates two important discrepan-

cies between the theoretical design conditions and the data obtained from the tests. First, none of the airfoils attain the design lift coefficient at the design angle (zero degrees) and second, the departure increases markedly with the lift coefficient. The departures may be important if variation from the ideal pressure distribution is rapid with change in lift coefficient. This effect, if great, would tend to cause lower drag and later critical speed for a narrow region near the design condition than is shown by these data. Similarly these departures also increase with the airfoil thickness.

These differences between the design conditions and the actual test results may be expected because of the simplifying assumptions of the thin airfoil theory. Theoretically it is assumed that the induced velocities are negligibly small as compared with the stream velocity. For thin airfoils at low lifts, this approximation is valid. With increases of lift or thickness, however, the induced velocities approach and sometimes exceed the stream velocity. Study of these effects appears to be very important in order to obtain the proper airfoil shapes for high lift coefficients and large thickness ratios. Deviations shown by the high lift and high thickness ratio airfoils in this series appear to indicate that the use of a single basic form is unwarranted if it is desired to obtain optimum airfoils for a wide range of lift coefficients and thickness distribution.

Theoretical pressure-distribution diagrams for the thicker airfoils show much greater slope of the pressure curve than is shown by the basic 16-009 form. Preliminary study indicates that increasing the leading-edge radius and the fullness of the airfoil between the leading edge and the maximum ordinate may lead to some considerable improvement over the thicker airfoils herein reported. Further investigation is now being conducted.

Comparison of airfoils.- Figures 19 and 20 illustrate the differences in aerodynamic characteristics between older propeller-blade sections and these new forms. At lower speeds (M = 0.45) the 3C8 airfoil appears to attain much higher maximum lift coefficient than the new airfoils. This is important in that the wider useful angle-of-attack range may frequently be required to prevent stalling of a propeller during the take-off. Over the normal flight range, however, and in most cases where rational choice of section can be made, the lower drag of

the new sections offers considerable opportunity to achieve higher efficiencies. The low drag attained by the N.A.C.A. 2409-34 airfoil developed from earlier tests in the 11-inch tunnel may appear surprising. Actually the type of flow for this airfoil approaches the flow that might be expected for the N.A.C.A. 16-309 airfoil.

The low drag common to most of the new airfoils is associated with more extensive regions of laminar flow in the boundary layer resulting from the rearward position of the point of maximum negative pressure. Unfortunately, however, the Reynolds Number is so low that effects of laminar separation may appear so that some pressure drag might occur. The small differences in drag between the envelope polar for the new airfoils and the 2409-34 airfoil are probably a result of this phenomenon. Actually the point of maximum negative pressure for the new airfoils is considerably farther aft than the corresponding point for the 2409-34 but, if laminar separation occurs early, nearly equal drag coefficients might be expected.

A detailed discussion of this phenomenon is given in an advance confidential report by E. N. Jacobs based on boundary-layer measurements for new airfoils tested in the low-turbulence wind tunnel.

At high speeds ($M = 0.75$) (fig. 20), the region for which the N.A.C.A. series 16 was designed, the superiority of the new airfoils is clear. The earlier onset of the compressibility effects for the older airfoils leads to early drag increases and lowered maximum lift coefficient. At speeds above M of 0.75 the use of the older sections appears unwarranted for any purpose.

Critical speed.- The variation of the critical speed with lift coefficient and with thickness is given in figures 21 and 22, respectively. These curves indicate that critical speeds exceeding the theoretical values were attained in the tests. In picking the test critical speeds the values were chosen on the basis of earlier experience that indicated some drag rise before shock occurred. If these speeds were chosen as the highest values reached before any appreciable drag increment occurred, the agreement with the theoretical curves would be very good. For comparison the critical speed of the 3C8 airfoil is plotted on figure 21. The difference between the new airfoils and the older forms is greater than shown by the curves because the 3C8 is 8 percent thick or 1 percent of the chord thinner than the 16-009 series.

Minimum drag.- Coefficients of minimum drag plotted against Reynolds Number are given in figures 23 and 24. The lowest drag coefficient was obtained for the 16-106 airfoil and is approximately 0.0026 at lower speeds increasing to approximately 0.0032 immediately below the critical speed. Of the 9 percent thick series designed to operate at various lift coefficients, the 16-109 appears to have the lowest drag. This is contrary to expectation because the symmetrical or basic form of the 16-009 would normally have the lowest minimum drag coefficient. The data were carefully checked and it appears that the lower drag of the 16-109 is real though as yet unexplained.

Comparison of the minimum drag coefficients for the 3C8, 2409-34, and the 16-209 airfoils is shown in figure 25. The higher critical speed for the 16-209 is apparent. The comparison as given directly by the figure is a little misleading because of the smaller thickness ratio for the 3C8. For equal thickness ratios the differences between the C series airfoils and the N.A.C.A. 16 series will be greater than shown.

Use of the data.- The envelope polars that may be drawn for the 16 series airfoils represent a new and much lower drag as well as higher critical speed attainable for the design of propeller-blade sections. Even though the angle-of-attack range is less than for the older sections, there will be numerous designs for which sufficient angle-of-attack range is given by the new sections. For high-speed, high-altitude aircraft, the advantages of the low drag and higher critical speed are of paramount importance and in these designs rational choice of section is of increasing importance. In many designs the diameter is fixed by considerations other than propeller efficiency. Thus the induced losses are fixed and propellers of highest efficiency can be had only by operating and designing the blade sections to work on the envelope polars. A further and most important matter in using new blade sections to achieve highest efficiency concerns the adaptation of the sections to older propeller designs. Optimum efficiency cannot be achieved by simply substituting the new sections for the old on a given design. The use of better blade sections permits the use of larger diameter and necessitates some plan-form changes. All of these should be considered in a design aimed at best efficiency using the new blade sections.

Langley Memorial Aeronautical Laboratory,
National Advisory Committee for Aeronautics,
Langley Field, Va., June 14, 1939.

REFERENCES

1. Stack, John: The Compressibility Burble. T.N. No. 543, N.A.C.A., 1935.

2. Jacobs, Eastman N.: Methods Employed in America for the Experimental Investigation of Aerodynamic Phenomena at High Speeds. Misc. Paper No. 42, N.A.C.A., 1936.

3. Stack, John, Lindsey, W. F., and Littell, Robert E.: The Compressibility Burble and the Effect of Compressibility on Pressures and Forces Acting on an Airfoil. T.R. No. 646, N.A.C.A., 1938.

4. Glauert, H.: The Elements of Aerofoil and Airscrew Theory. Cambridge University Press, 1926.

5. Theodorsen, Theodore: Theory of Wing Sections of Arbitrary Shape. T.R. No. 411, N.A.C.A., 1931.

6. Stack, John, and von Doenhoff, A. E.: Tests of 16 Related Airfoils at High Speeds. T.R. No. 492, N.A.C.A., 1934.

7. Stack, John: The N.A.C.A. High-Speed Wind Tunnel and Tests of Six Propeller Sections. T.R. No. 463, N.A.C.A., 1933.

8. Jacobs, Eastman N., Ward, Kenneth E., and Pinkerton, Robert M.: The Characteristics of 78 Related Airfoil Sections from Tests in the Variable-Density Wind Tunnel. T.R. No. 460, N.A.C.A., 1933.

Table I, heading:

"Series ∉ 07 Camber Line Ordinates" should read

"Series 16 ∉ 07 Camber Line Ordinates"

16

TABLE I

Series ℓ 07 Camber Line Ordinates

$C_L = 1.0$

All values measured in percent chord from chord line

Station	Ordinate*	Slope
0	0	0.62234
1.25	.535	.34771
2.5	.930	.29155
5	1.580	.23432
7.5	2.120	.19993
10	2.587	.17486
15	3.364	.13804
20	3.982	.11032
25	4.475	.08743
30	4.861	.06743
40	5.356	.03227
50	5.516	0
60	5.356	.03227
70	4.861	.06743
80	3.982	.11032
90	2.587	.17486
95	1.580	.23432
100	0	.62234

These camber ordinates are the same as those for low drag airfoil $a = 1.0$ RBE 4/21/44

* Multiply by value of C_L for other design lift coefficients

TABLE II

Thickness Ordinates for Thickness of 9* Percent of Chord

All values measured in percent of chord from ℄ perpendicular to camber line

Station	Series 16 Ordinates	07-009 Ordinates
0	0	0
1.25	.969	1.23
2.5	1.354	1.67
5	1.882	2.19
7.5	2.274	2.58
10	2.593	2.90
15	3.101	3.41
20	3.498	3.79
25		4.07
30	4.063	4.27
40	4.391	4.46
50	4.500	4.50
60	4.376	4.37
70	3.952	4.00
80	3.149	3.34
90	1.888	1.91
95	1.061	1.00
100	.090	.09
Slope of radius through end of chord	= 0.62234 C_L	
Series 16 L.E. radius = 0.396 $(t/.09)^2$		

*For other thicknesses (t, in percent) multiply series 16 ordinates by t/.09

FIGURE LEGENDS

Figure 1.- Basic airfoil forms.

Figure 2.- Profiles for high critical speeds.

Figure 3.- Comparison of minimum drag obtained by various methods.

(a) Polar plots.
(b) Lift and moment data.
Figure 4.- Airfoil characteristics. N.A.C.A. series 16-009. M = 0.30.

(a) Polar plots.
(b) Lift and moment data.
Figure 5.- Airfoil characteristics. N.A.C.A. series 16-009. M = 0.45.

(a) Polar plots.
(b) Lift and moment data.
Figure 6.- Airfoil characteristics. N.A.C.A. series 16-009. M = 0.60.

(a) Polar plots.
(b) Lift and moment data.
Figure 7.- Airfoil characteristics. N.A.C.A. series 16-009. M = 0.70.

(a) Polar plots.
(b) Lift and moment data.
Figure 8.- Airfoil characteristics. N.A.C.A. series 16-009. M = 0.75.

(a) Polar plots.
(b) Lift and moment data.
Figure 9.- Airfoil characteristics. N.A.C.A. series 16-500. M = 0.30.

(a) Polar plots.
(b) Lift and moment data.
Figure 10.- Airfoil characteristics. N.A.C.A. series 16-500. M = 0.45.

(a) Polar plots.
(b) Lift and moment data.
Figure 11.- Airfoil characteristics. N.A.C.A. series 16-500. M = 0.60.

(a) Polar plots.
(b) Lift and moment data.
Figure 12.- Airfoil characteristics. N.A.C.A. series 16-500. M = 0.70.

(a) Polar plots.
(b) Lift and moment data.
Figure 13.- Airfoil chatacteristics. N.A.C.A. series 16-500. M = 0.75.

(a) Polar plots.
(b) Lift and moment data.
Figure 14.- Airfoil characteristics. N.A.C.A. series 16-000. M = 0.30.

(a) Polar plots.
(b) Lift and moment data.
Figure 15.- Airfoil characteristics. N.A.C.A. series 16-000. M = 0.45.

(a) Polar plots
(b) Lift and moment data.
Figure 16.- Airfoil characteristics. N.A.C.A. series 16-000. M = 0.60.

(a) Polar plots.
(b) Lift and moment data.
Figure 17.- Airfoil characteristics. N.A.C.A. series 16-000. M = 0.70.

(a) Polar plots.
(b) Lift and moment data.
Figure 18.- Airfoil characteristics. N.A.C.A. series 16-000. M = 0.75.

Figure 19.- Comparison of N.A.C.A. airfoils. M = 0.45.

Figure 20.-Comparison of N.A.C.A. airfoils. M = 0.75.

Figure 21.-Airfoil critical speed. Variation with lift.

Figure 22.- Airfoil critical speed. Variation with thickness.

Figure 23.- Minimum drag for the N.A.C.A. airfoils, series 16-009.

Figure 24.- Minimum drag for the N.A.C.A. airfoils, series 16-500.

Figure 25.-Comparison of airfoil drag coefficients.

N.A.C.A.

Figs. 1,3,25

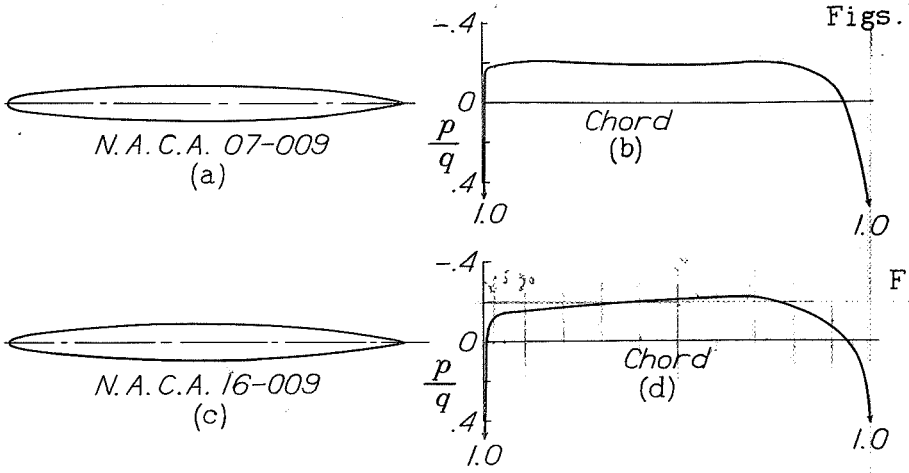

Figure 1

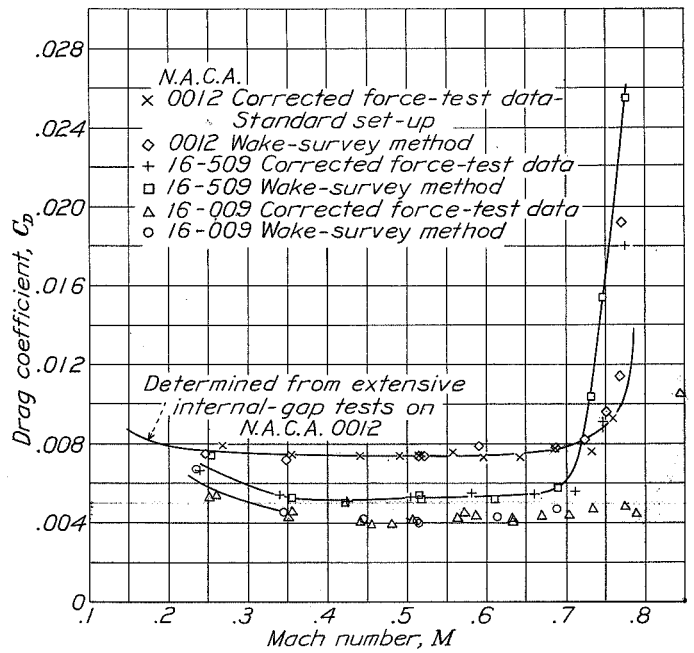

Figure 3

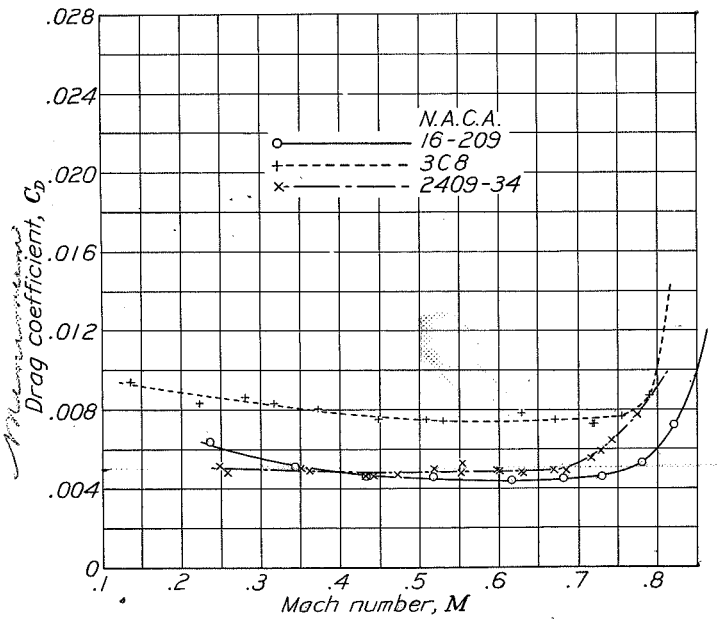

Figure 25

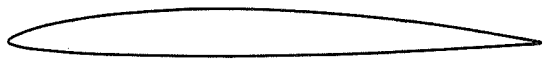

N.A.C.A. 2409-34

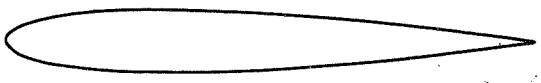

N.A.C.A. 0012

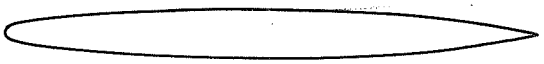

N.A.C.A. 07-009

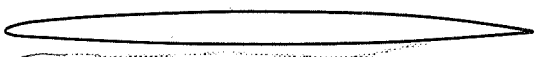

N.A.C.A. 16-106

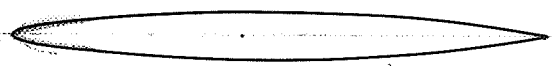

N.A.C.A. 16-009

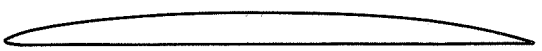

N.A.C.A. 16-506

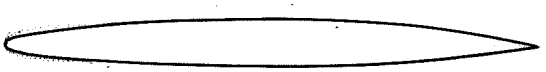

N.A.C.A. 16-109

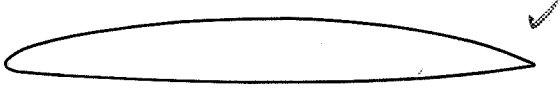

N.A.C.A. 16-512

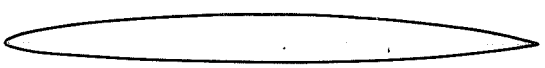

N.A.C.A. 16-209

N.A.C.A. 16-515

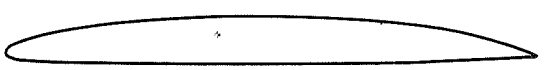

N.A.C.A. 07-509

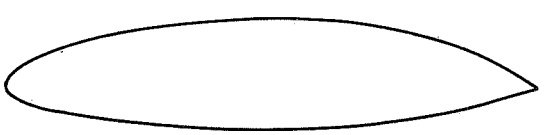

N.A.C.A. 16-521

N.A.C.A. 16-509

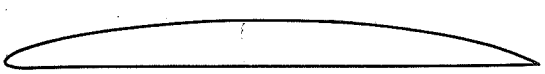

N.A.C.A. 16-709

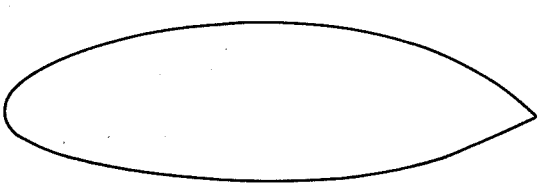

N.A.C.A. 16-530

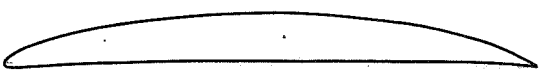

N.A.C.A. 16-1009

Figure 2

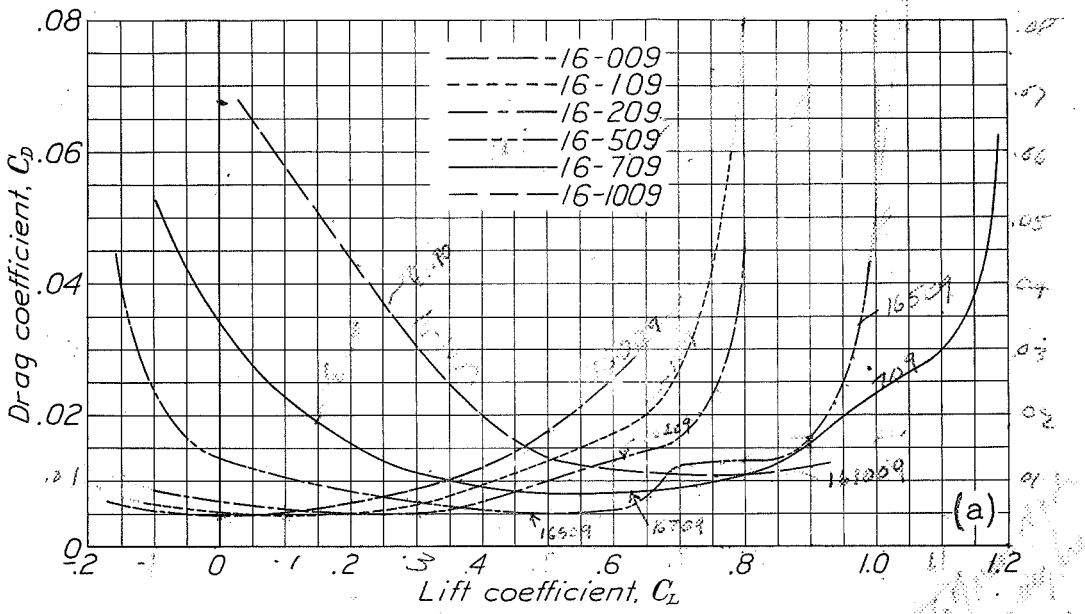
16-009
16-109
16-209
16-509
16-709
16-1009
Drag coefficient, C_D
Lift coefficient, C_L
(a)

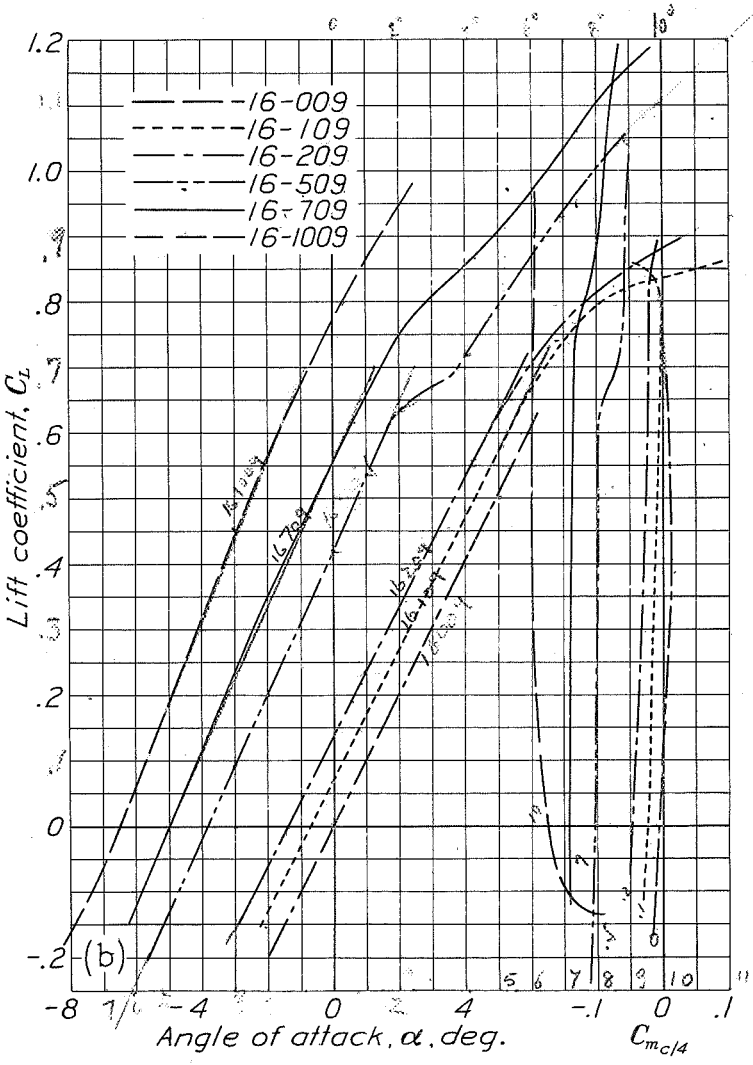
16-009
16-109
16-209
16-509
16-709
16-1009
Lift coefficient, C_L
Angle of attack, α, deg.
$C_{m_{c/4}}$
(b)

Figure 4

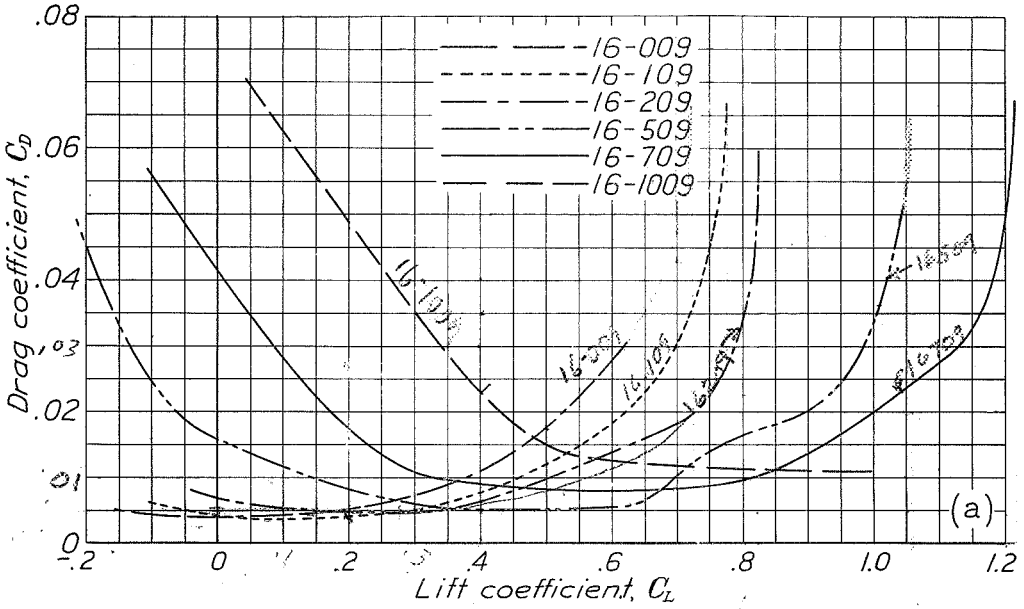
16-009
16-109
16-209
16-509
16-709
16-1009
Drag coefficient, C_D
Lift coefficient, C_L
(a)

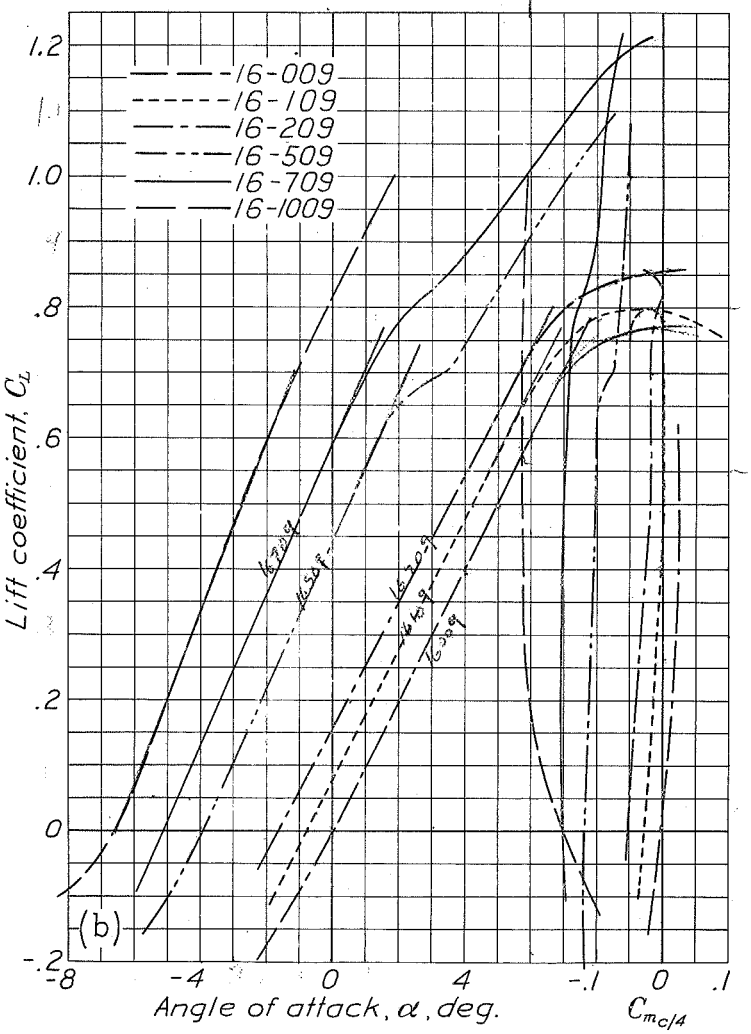
16-009
16-109
16-209
16-509
16-709
16-1009
Lift coefficient, C_L
Angle of attack, α, deg.
$C_{m_{c/4}}$
(b)

Figure 5

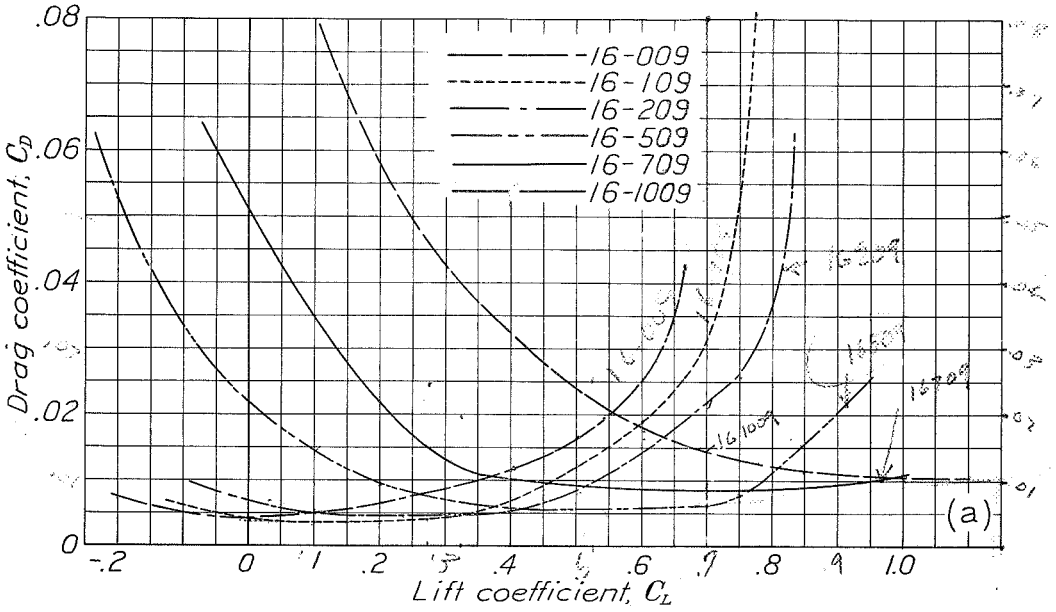
16-009
16-109
16-209
16-509
16-709
16-1009
Drag coefficient, C_D
Lift coefficient, C_L
(a)

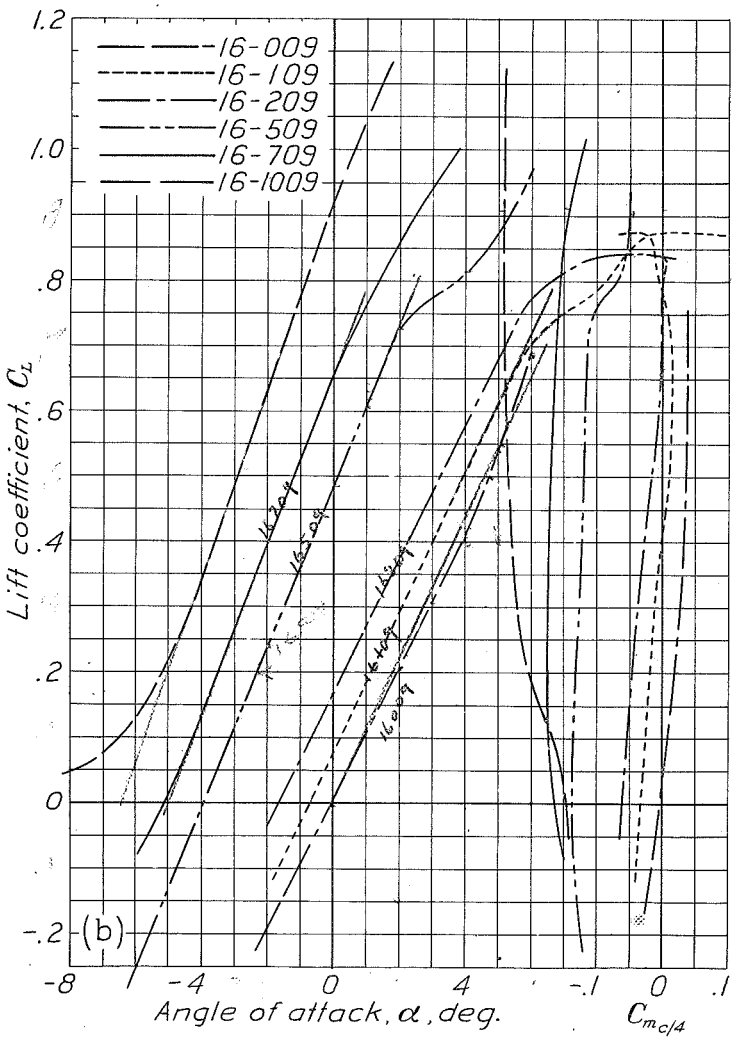
16-009
16-109
16-209
16-509
16-709
16-1009
Lift coefficient, C_L
Angle of attack, α, deg.
$C_{m_{c/4}}$
(b)

Figure 6

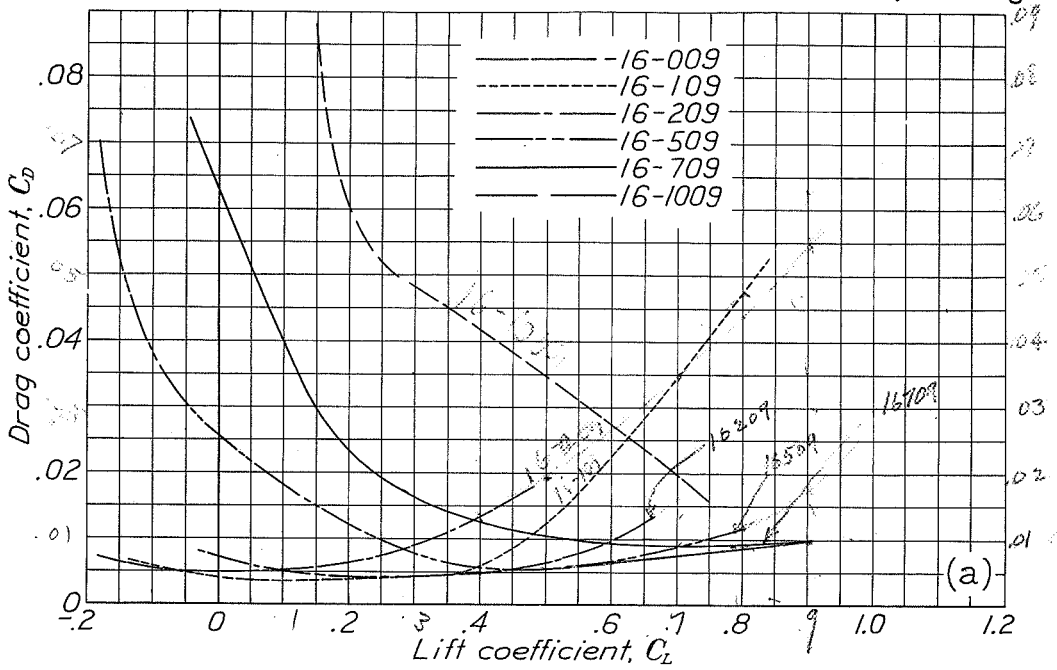
16-009
16-109
16-209
16-509
16-709
16-1009
Drag coefficient, C_D
Lift coefficient, C_L
(a)

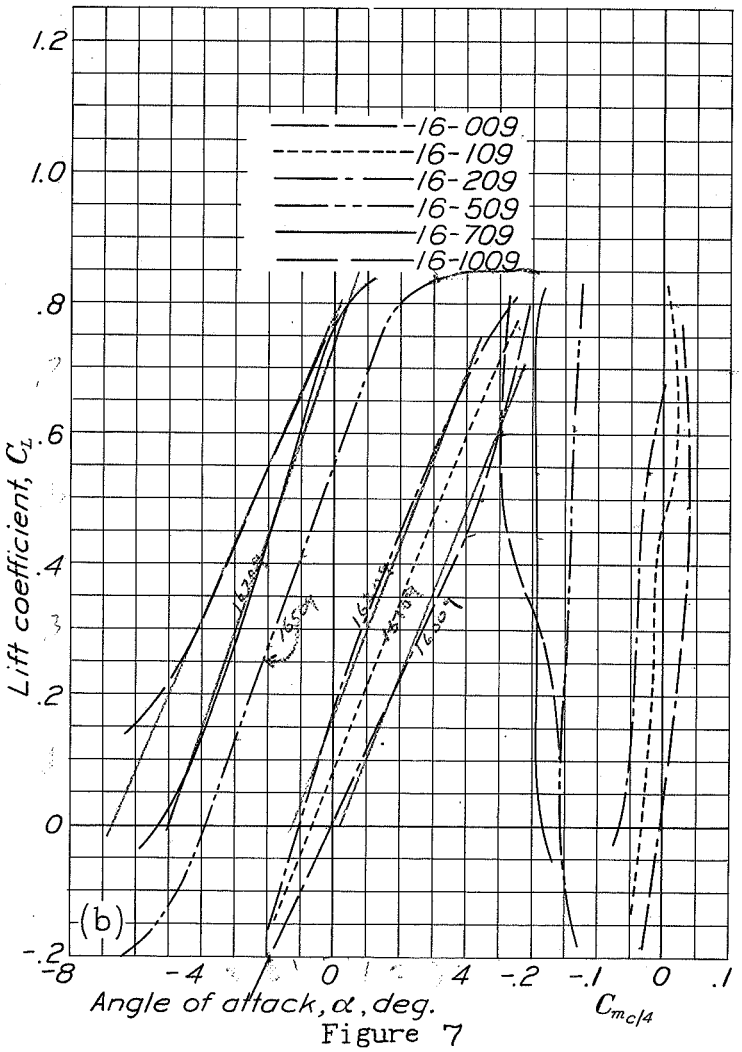
16-009
16-109
16-209
16-509
16-709
16-1009
Lift coefficient, C_L
Angle of attack, α, deg.
$C_{m_{c/4}}$
(b)

Figure 7

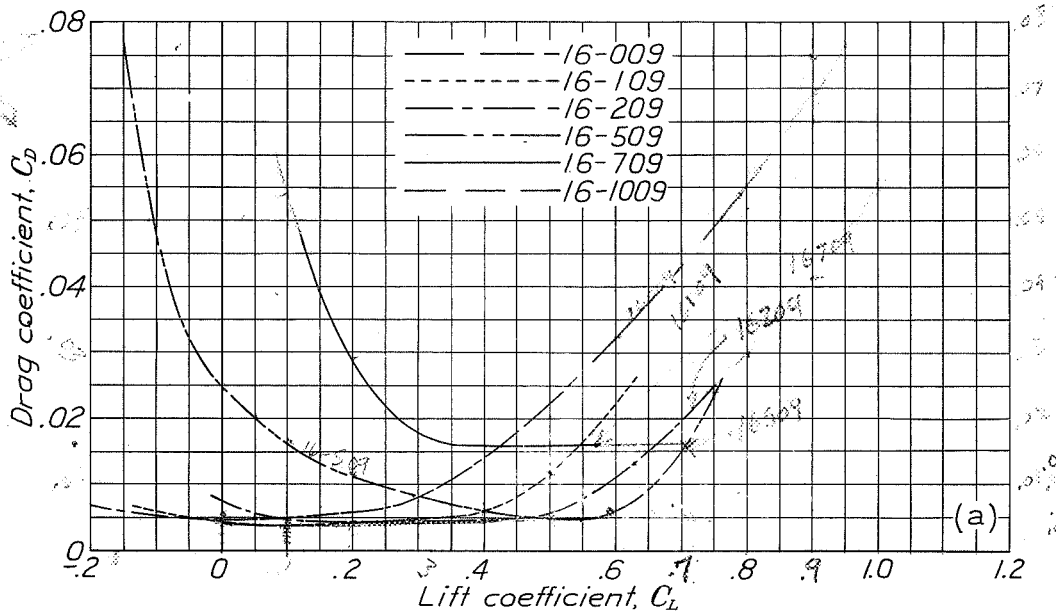
16-009
16-109
16-209
16-509
16-709
16-1009
Drag coefficient, C_D
.08
.06
.04
.02
0
-.2
0
.2
.4
.6
.8
1.0
1.2
Lift coefficient, C_L
(a)

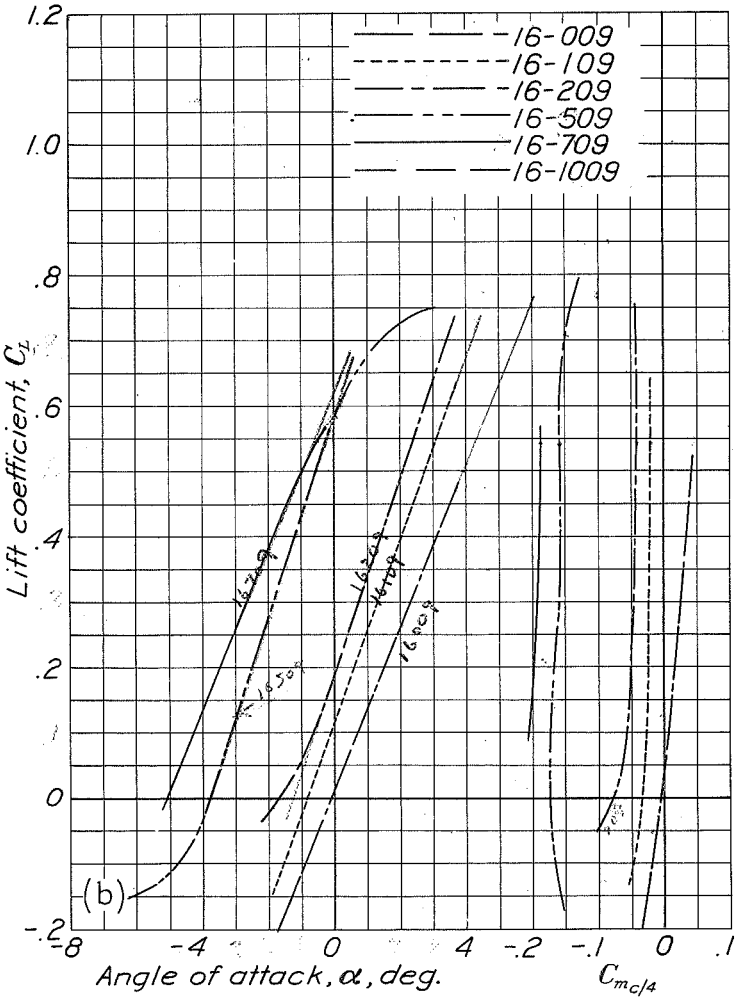
16-009
16-109
16-209
16-509
16-709
16-1009
Lift coefficient, C_L
1.2
1.0
.8
.6
.4
.2
0
-.2
-8
-4
0
4
Angle of attack, α, deg.
-.2
-.1
0
.1
$C_{m_{c/4}}$
(b)

Figure 8

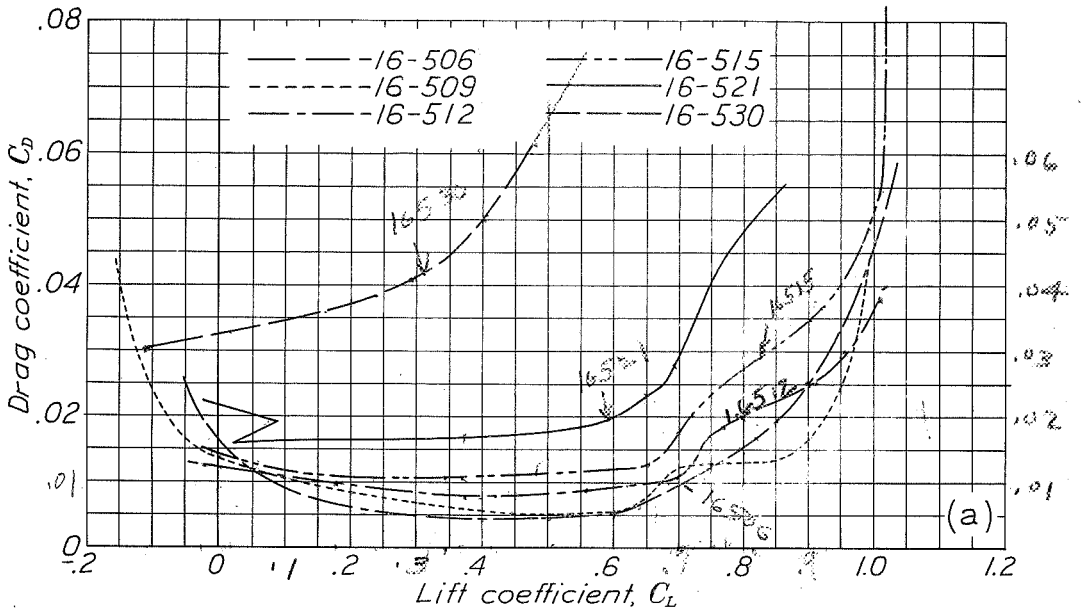
16-506
16-509
16-512
16-515
16-521
16-530
Drag coefficient, C_D
Lift coefficient, C_L
(a)

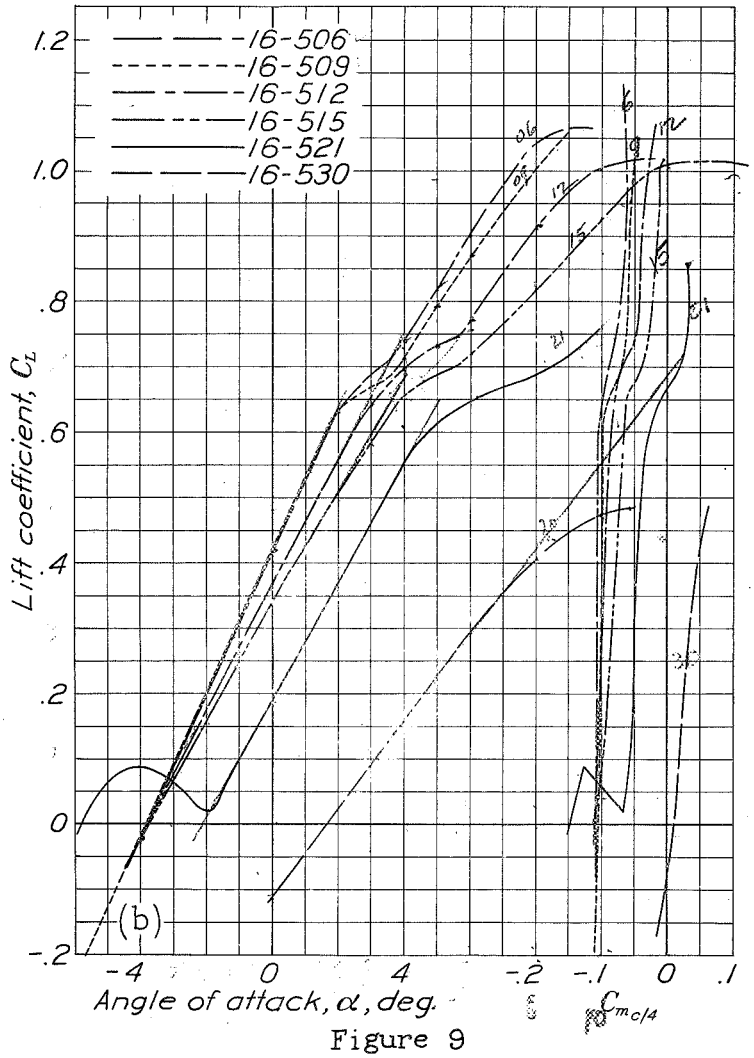
16-506
16-509
16-512
16-515
16-521
16-530
Lift coefficient, C_L
Angle of attack, α, deg.
$C_{m_{c/4}}$
(b)

Figure 9

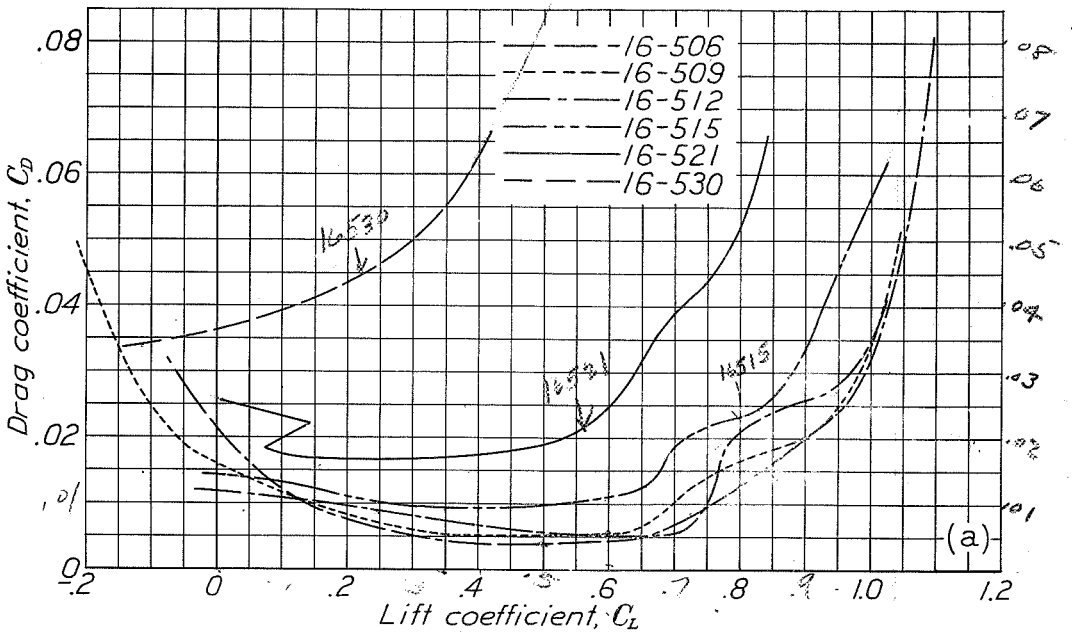
16-506
16-509
16-512
16-515
16-521
16-530
Drag coefficient, C_D
Lift coefficient, C_L
(a)

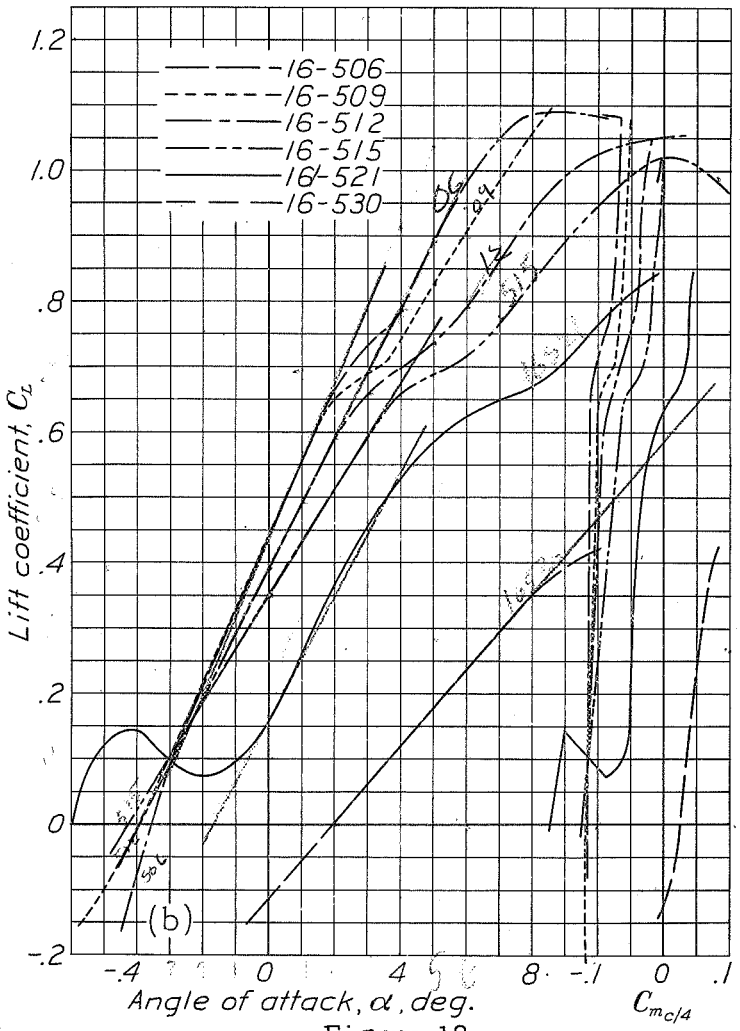
16-506
16-509
16-512
16-515
16-521
16-530
Lift coefficient, C_L
Angle of attack, α, deg.
$C_{m_{c/4}}$
(b)

Figure 10

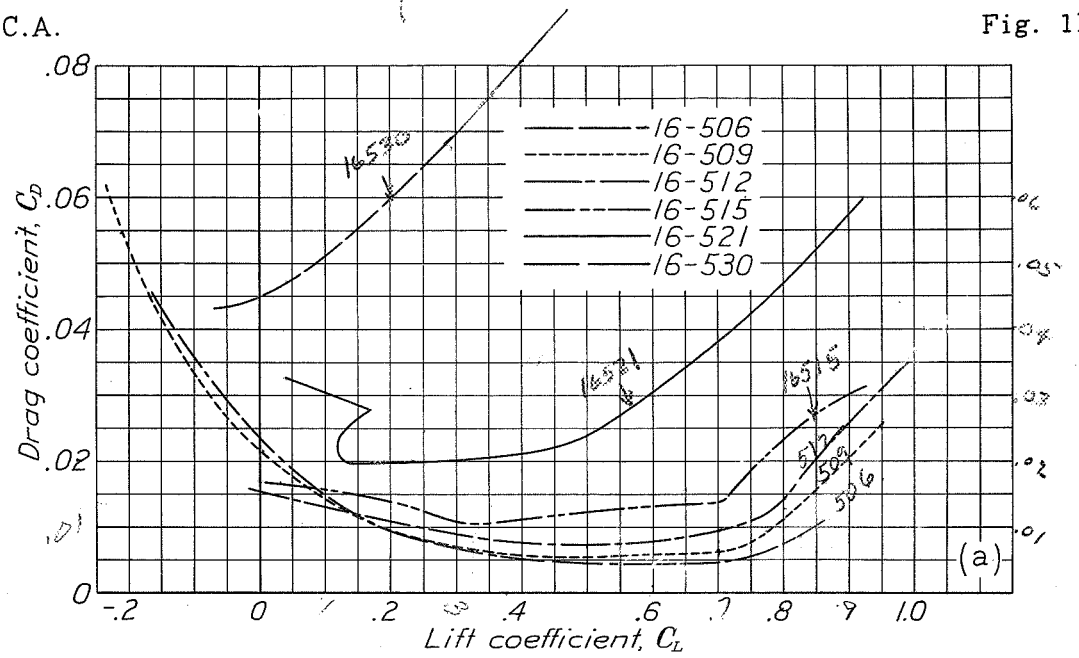
16-506
16-509
16-512
16-515
16-521
16-530
Drag coefficient, C_D
Lift coefficient, C_L
(a)

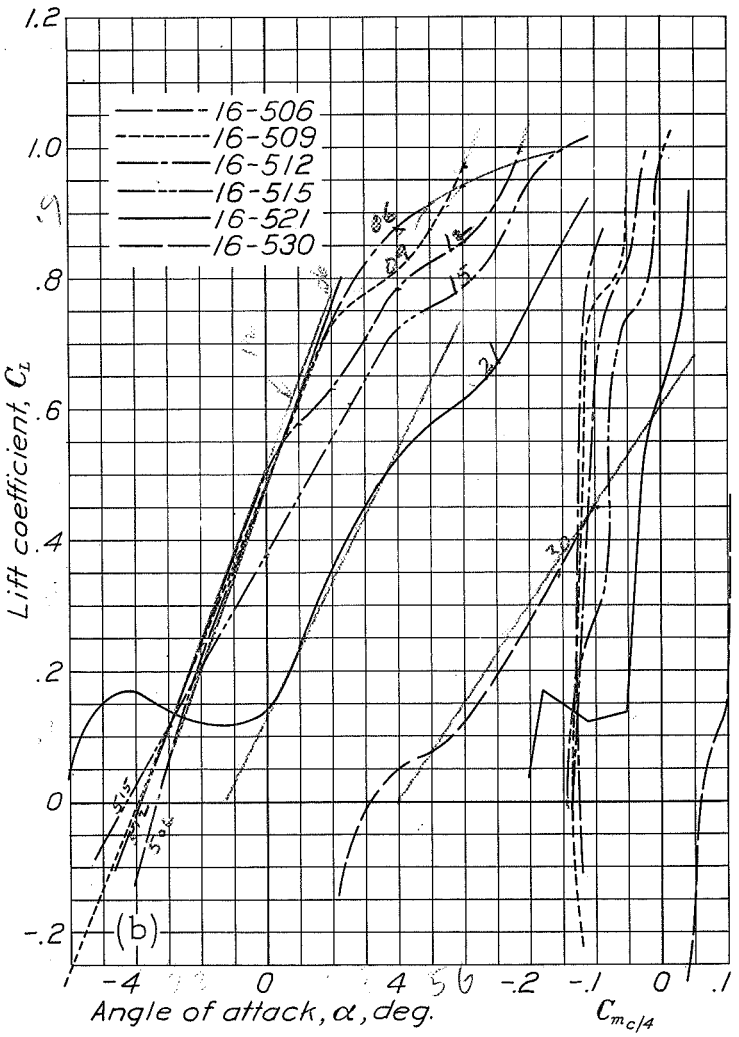
16-506
16-509
16-512
16-515
16-521
16-530
Lift coefficient, C_L
Angle of attack, α, deg.
$C_{m_{c/4}}$
(b)

Figure 11

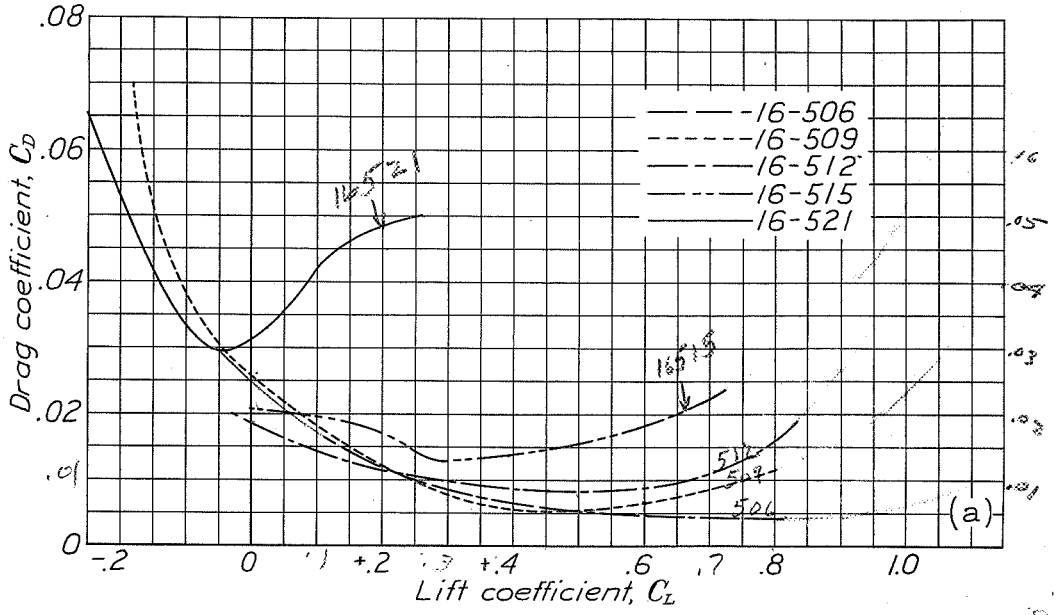
16-506
16-509
16-512
16-515
16-521
Drag coefficient, C_D
Lift coefficient, C_L
(a)

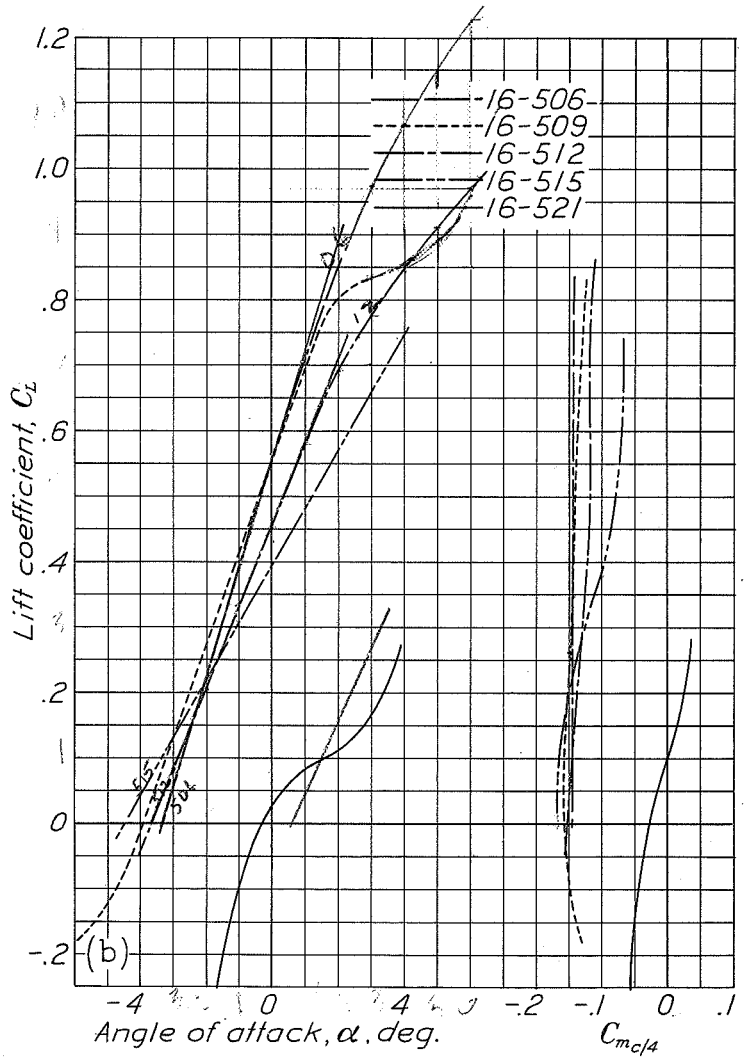
16-506
16-509
16-512
16-515
16-521
Lift coefficient, C_L
Angle of attack, α, deg.
$C_{m_{c/4}}$
(b)

Figure 12

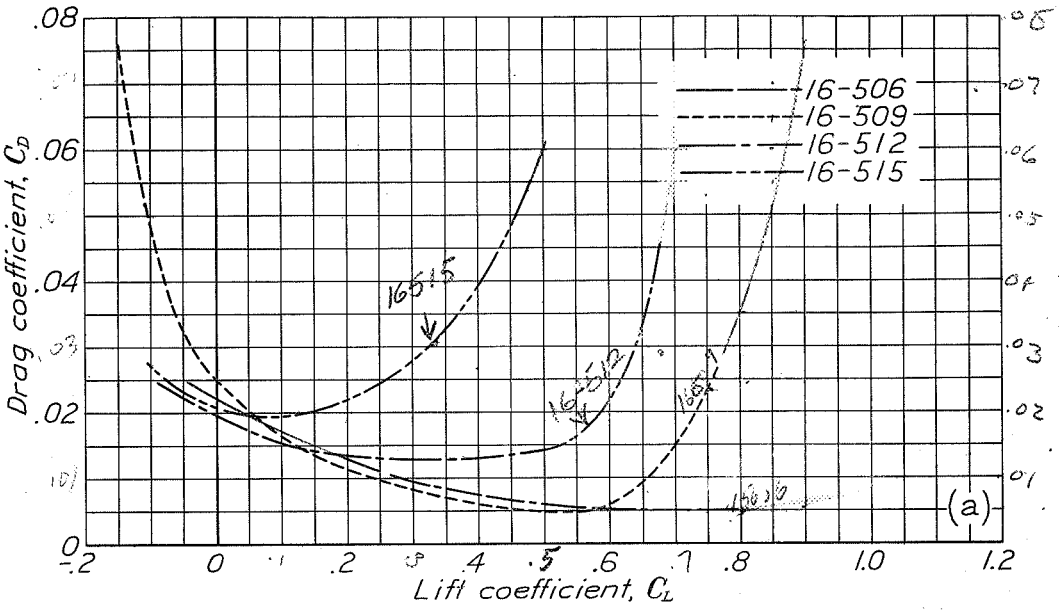
16-506
16-509
16-512
16-515
Drag coefficient, C_D
Lift coefficient, C_L
(a)

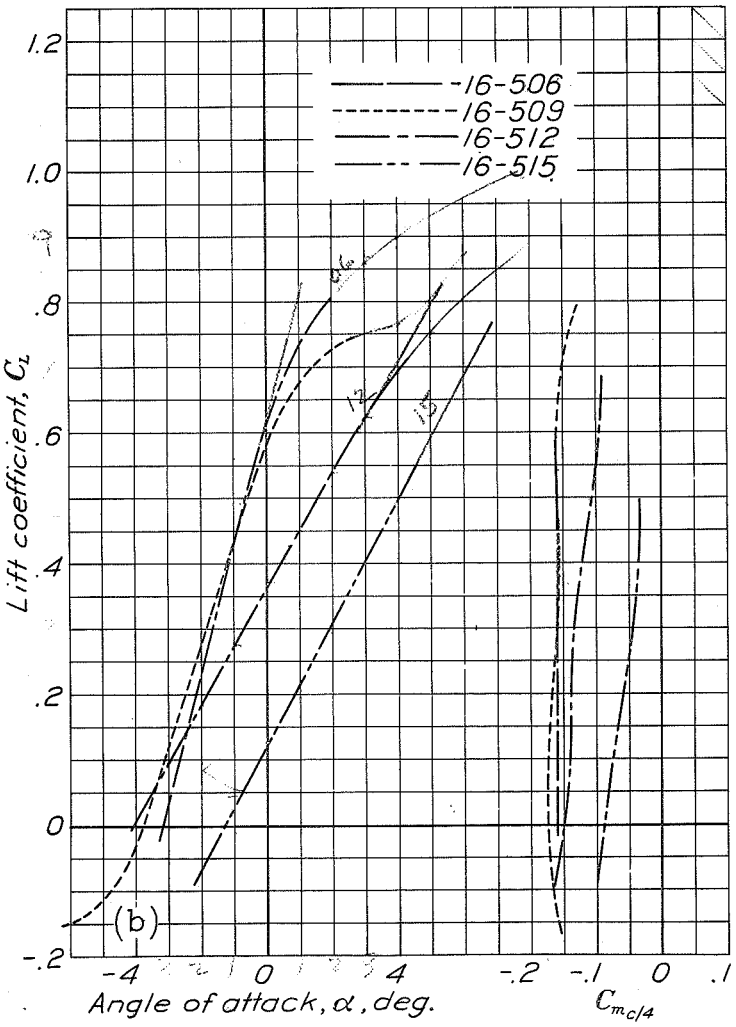
16-506
16-509
16-512
16-515
Lift coefficient, C_L
Angle of attack, α, deg.
$C_{m_{c/4}}$
(b)

Figure 13

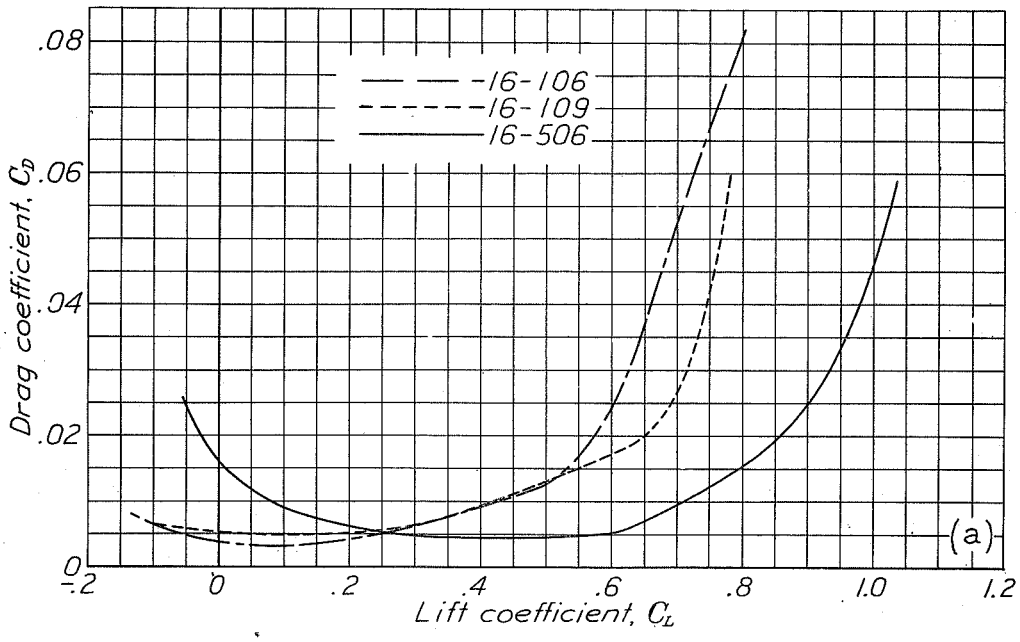
.08
.06
.04
.02
0
Drag coefficient, C_D
-.2
0
.2
.4
.6
.8
1.0
1.2
Lift coefficient, C_L
16-106
16-109
16-506
(a)

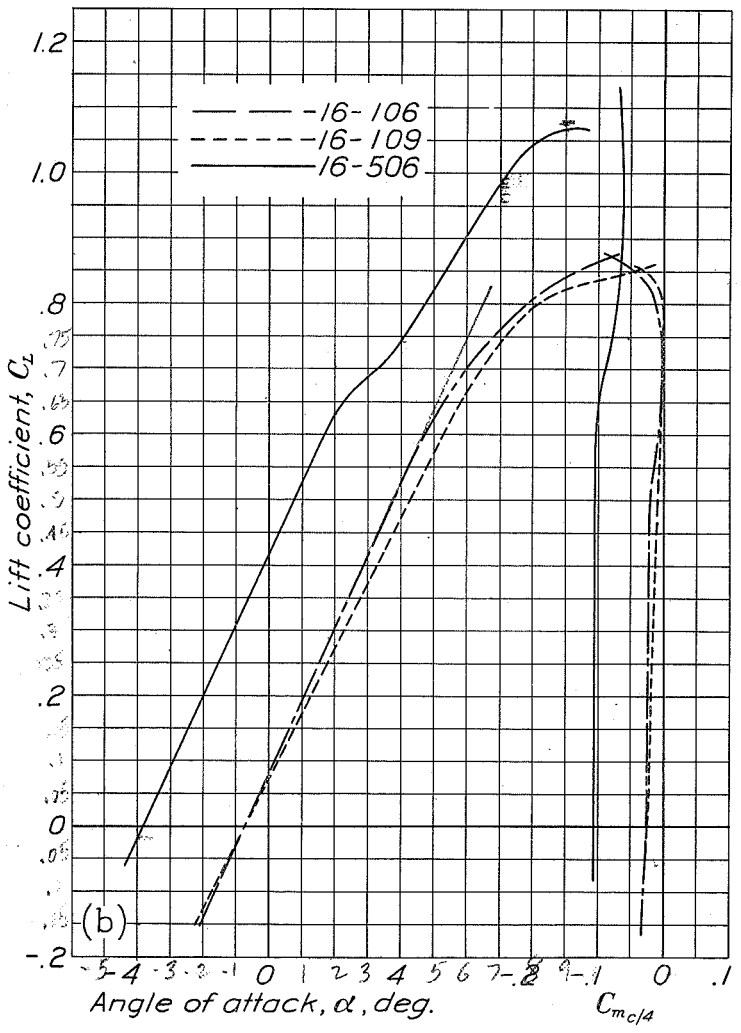
1.2
1.0
.8
.6
.4
.2
0
-.2
Lift coefficient, C_L
-5 -4 -3 -2 -1 0 1 2 3 4 5 6 7 8 9
Angle of attack, α, deg.
-.1
0
.1
$C_{m_{c/4}}$
16-106
16-109
16-506
(b)

Figure 14

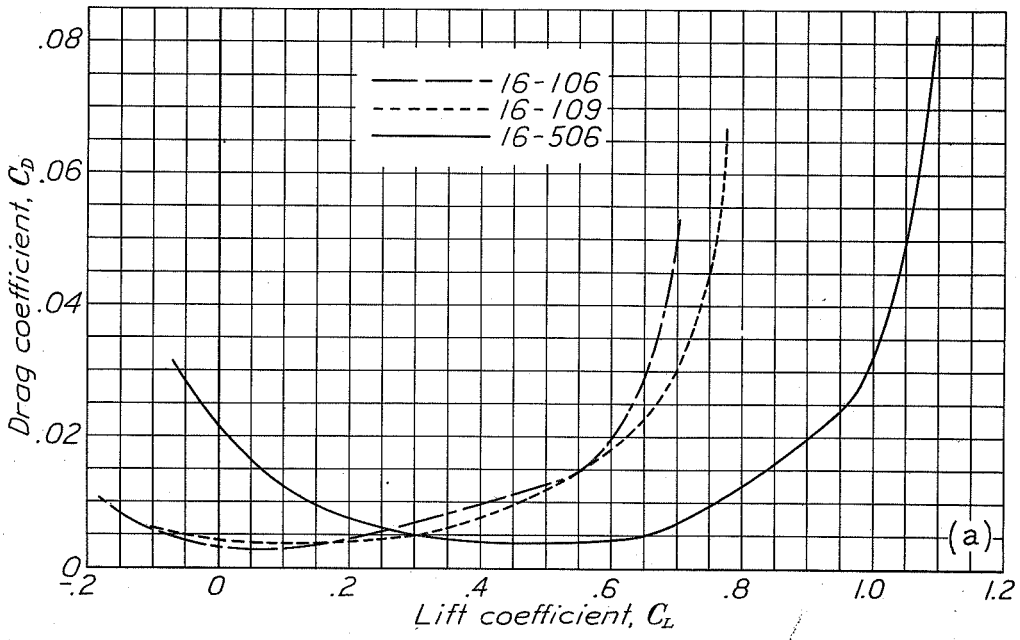
16-106
16-109
16-506
Drag coefficient, C_D
.08
.06
.04
.02
0
-.2
0
.2
.4
.6
.8
1.0
1.2
Lift coefficient, C_L
(a)

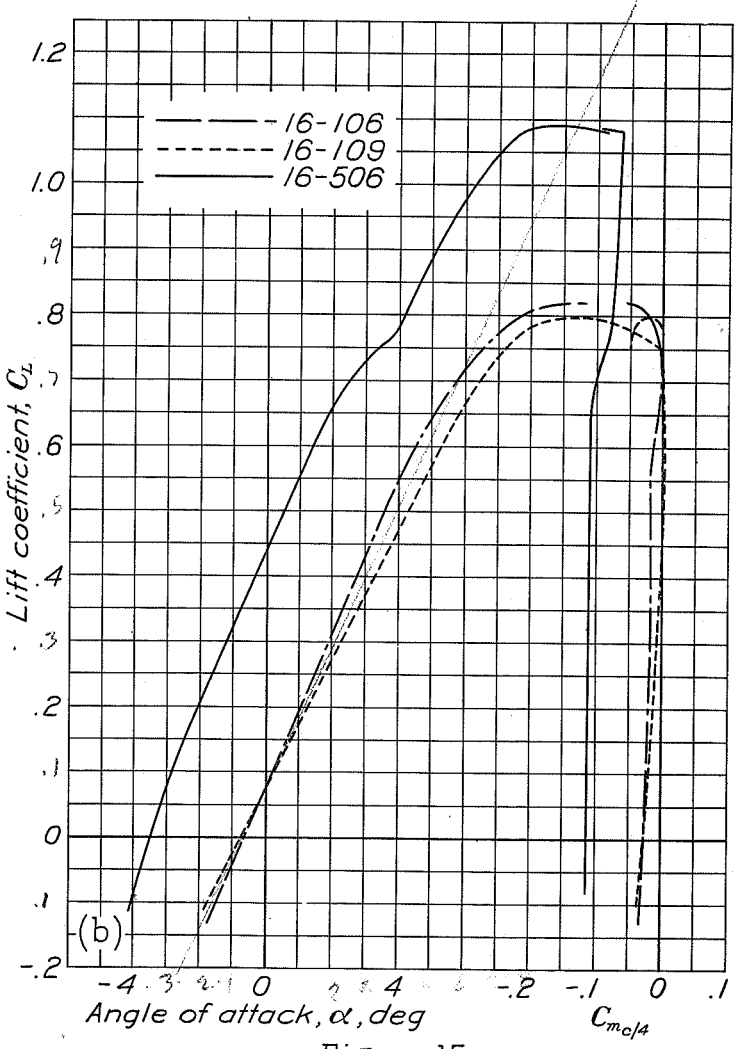
16-106
16-109
16-506
Lift coefficient, C_L
1.2
1.0
.9
.8
.6
.4
.2
0
-.2
-4
0
4
-.2
-.1
0
.1
Angle of attack, α, deg
$C_{m_{c/4}}$
(b)

Figure 15

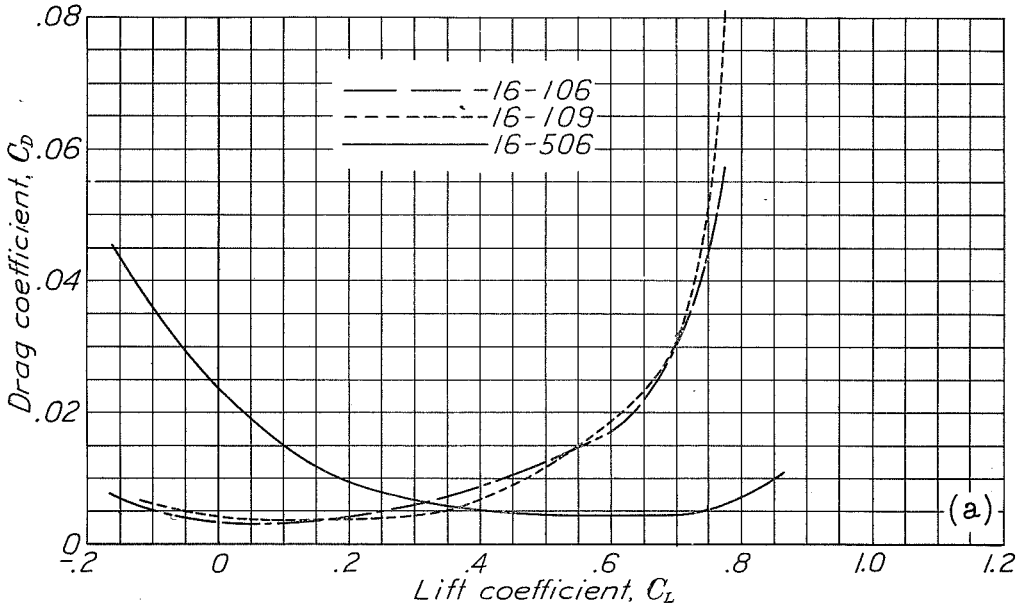
.08
.06
.04
.02
0
Drag coefficient, C_D
16-106
16-109
16-506
(a)
-.2
0
.2
.4
.6
.8
1.0
1.2
Lift coefficient, C_L

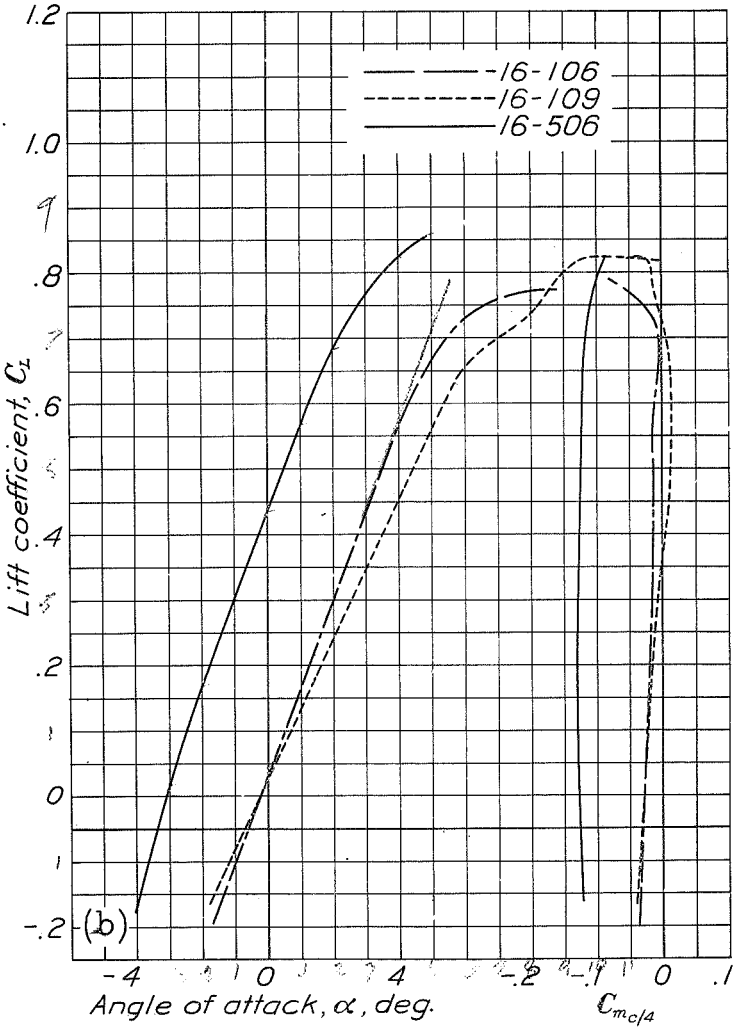
1.2
1.0
.8
.6
.4
.2
0
-.2
Lift coefficient, C_L
16-106
16-109
16-506
(b)
-4
0
4
-.2
-.1
0
.1
Angle of attack, α, deg.
$C_{m_{c/4}}$

Figure 16

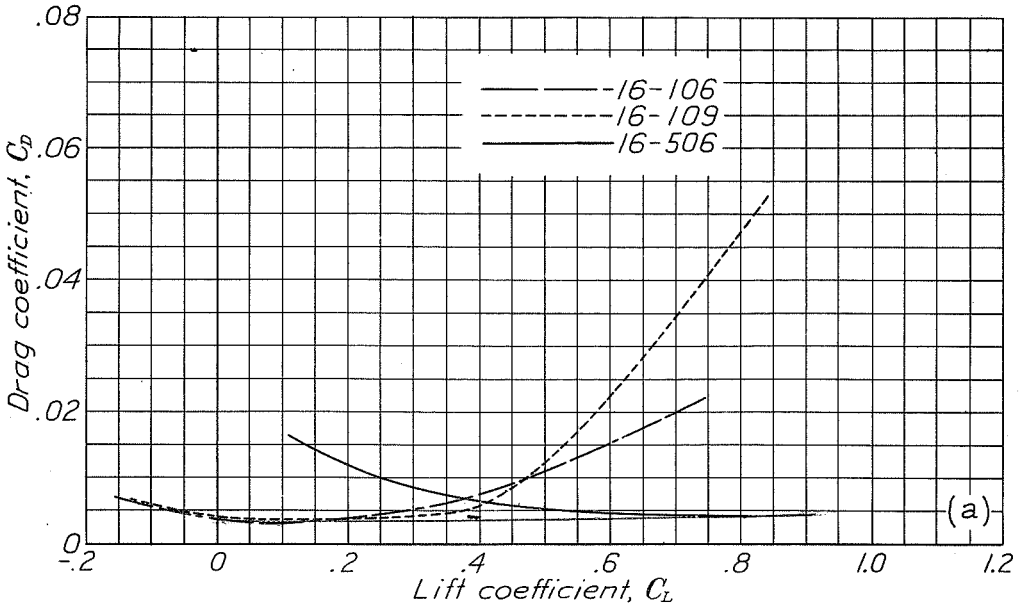
.08
.06
.04
.02
0
Drag coefficient, C_D
16-106
16-109
16-506
(a)
-.2
0
.2
.4
.6
.8
1.0
1.2
Lift coefficient, C_L

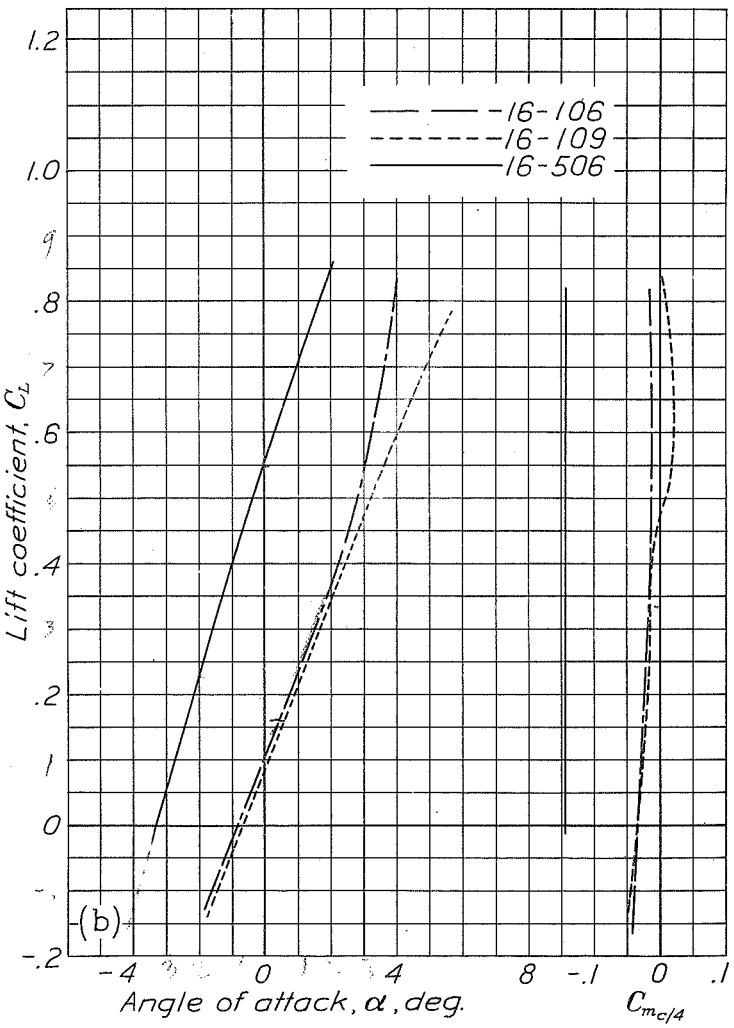
1.2
1.0
.8
.6
.4
.2
0
-.2
Lift coefficient, C_L
16-106
16-109
16-506
(b)
-4
0
4
8
-.1
0
.1
Angle of attack, α, deg.
$C_{m_{c/4}}$

Figure 17

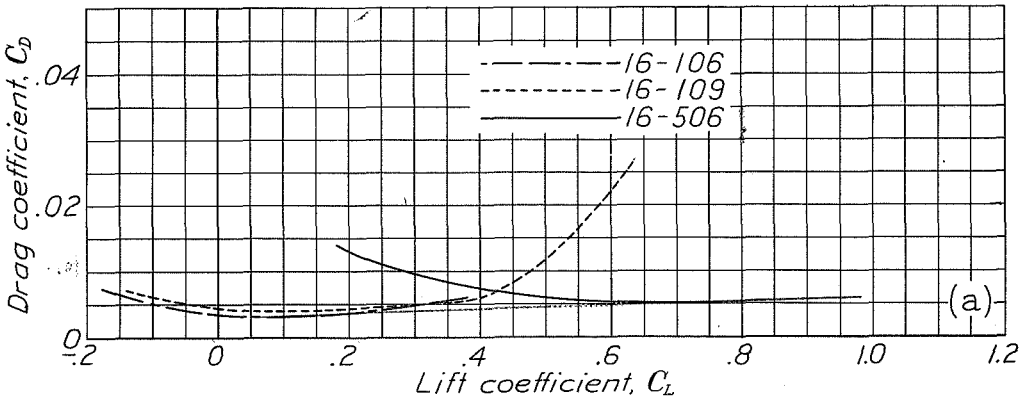
Drag coefficient, C_D
.04
.02
0
16-106
16-109
16-506
(a)
-.2
0
.2
.4
.6
.8
1.0
1.2
Lift coefficient, C_L

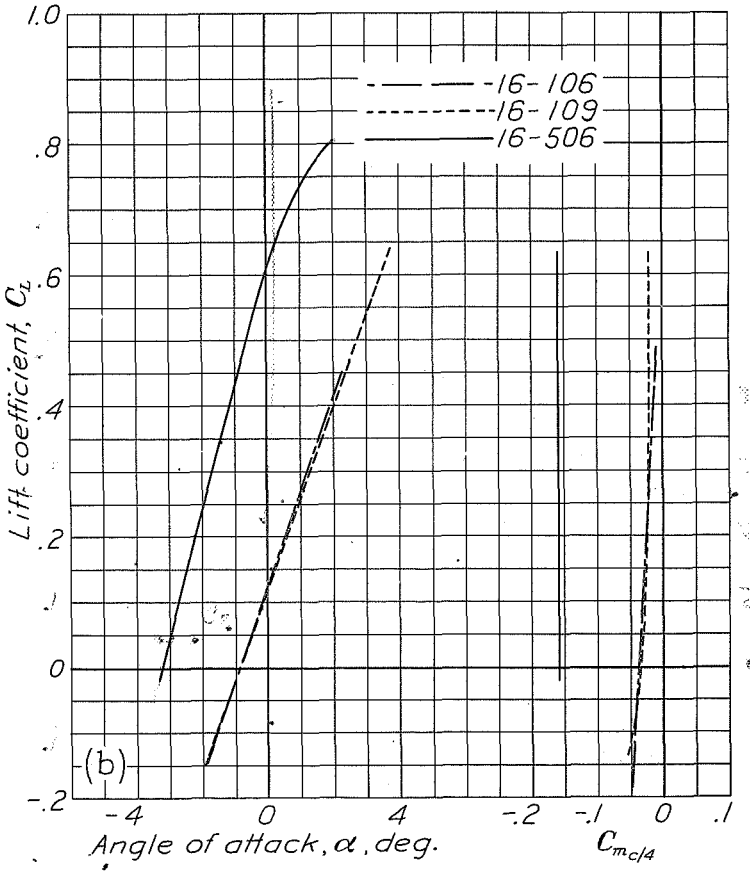
Lift coefficient, C_L
1.0
.8
.6
.4
.2
0
-.2
16-106
16-109
16-506
(b)
-4
0
4
Angle of attack, α, deg.
-.2
-.1
0
.1
$C_{m_{c/4}}$

Figure 18

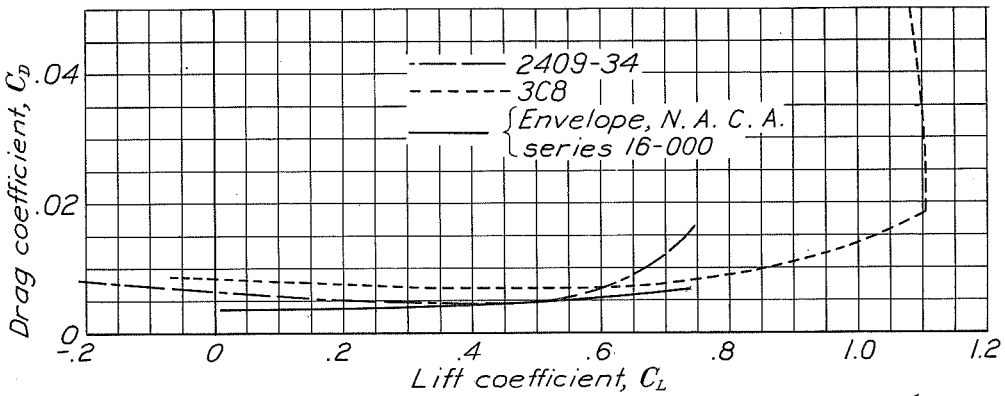

Figure 19

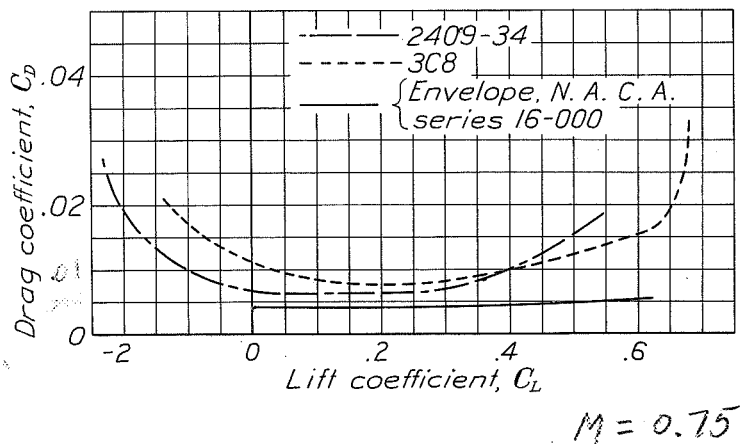

2409-34 results from earlier tests in 11" HST (Camp 8)

Figure 20

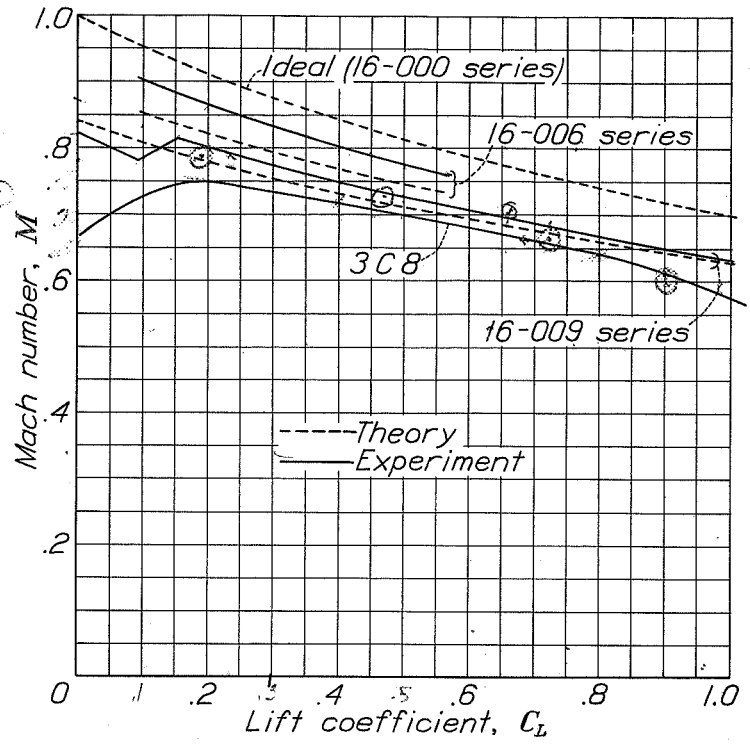

Figure 21

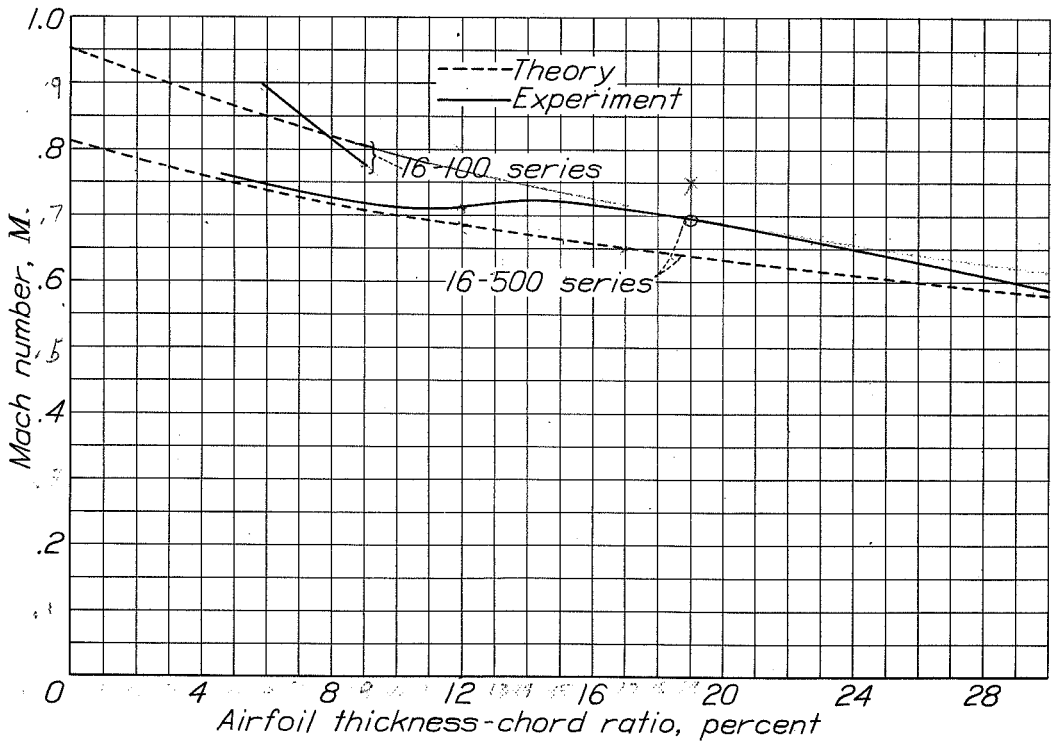

Figure 22

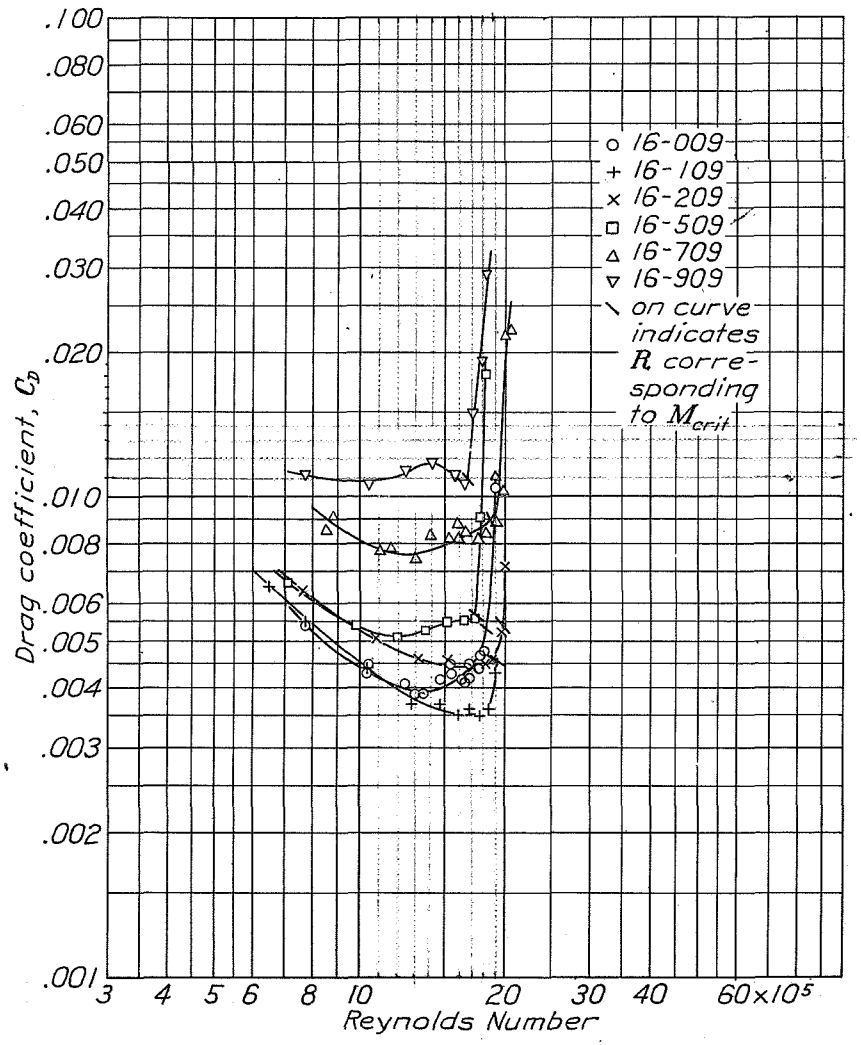

Figure 23

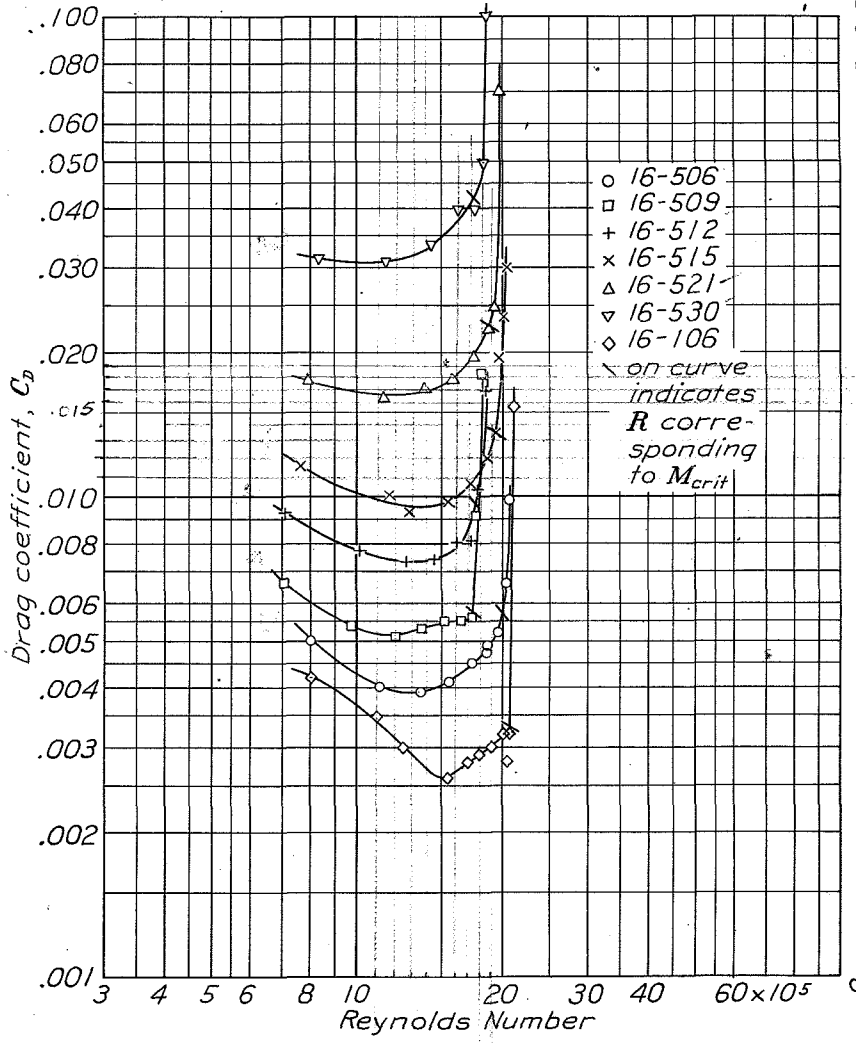

Figure 24